

LATERAL BUCKLING OF OVERHANGING BEAMS

**A THESIS SUBMITTED TO
THE GRADUATE SCHOOL OF NATURAL AND APPLIED SCIENCES
OF
MIDDLE EAST TECHNICAL UNIVERSITY**

BY

KEREM MURAT ÖZDEMİR

**IN PARTIAL FULFILLMENT OF THE REQUIREMENTS
FOR
THE DEGREE OF MASTER OF SCIENCE
IN
CIVIL ENGINEERING**

AUGUST 2005

Approval of the Graduate School of Natural and Applied Sciences

Prof. Dr. Canan Özgen
Director

I certify that this thesis satisfies all the requirements as a thesis for the degree of Master of Science

Prof. Dr. Erdal Çokca
Head of Department

This is to certify that we have read this thesis and that in our opinion it is fully adequate, in scope and quality, as a thesis for the degree of Master of Science.

Assoc. Prof. Dr. Cem Topkaya
Supervisor

Examining Committee Members

Prof. Dr. Güney Özcebe	(METU, CE)	_____
Assoc. Prof. Dr. Cem Topkaya	(METU, CE)	_____
Assoc. Prof. Dr. Ahmet Yakut	(METU, CE)	_____
Assoc. Prof. Dr. Uğurhan Akyüz	(METU, CE)	_____
Volkan Aydoğan (M.S.)	(PROYA)	_____

I hereby declare that all information in this document has been obtained and presented in accordance with academic rules and ethical conduct. I also declare that, as required by these rules and conduct, I have fully cited and referenced all material and results that are not original to this work.

Name, Last name : Kerem Murat Özdemir

Signature :

ABSTRACT

LATERAL BUCKLING OF OVERHANGING BEAMS

Özdemir, Kerem Murat

M.S., Department of Civil Engineering

Supervisor: Assoc. Prof. Dr. Cem Topkaya

August 2005, 65 pages

Lateral torsional buckling should be taken into account during the design of overhanging steel beams. One special type of overhanging beams is the crane trolley monorails. Lateral buckling of overhanging monorails under idealized loading and boundary conditions has been studied in the past using classical mathematical procedures. This thesis aims to present a detailed investigation of overhanging monorails using finite element analysis. Effects of different loading and boundary conditions were studied in detail. It was found out that the location of loading and supports on the cross section have significant effects on the buckling capacity. Beams having different warping and torsional properties were analyzed. The effects of cross section distortion on buckling capacity were investigated for beams with single and double overhangs. The reduction in capacity due to cross section distortion has been quantified. Based on the analysis results simple design recommendations were developed for lateral buckling of overhanging monorails and they are presented herein.

Keywords: Lateral Torsional Buckling, Overhanging Beams, Crane Trolley Monorails

ÖZ

ÜSTTEN ASILI KİRİŞLERİN YANAL BURKULMASI

Özdemir, Kerem Murat

Yüksek Lisans, İnşaat Mühendisliği Bölümü

Tez Yöneticisi: Doç. Dr. Cem Topkaya

Ağustos 2005, 65 sayfa

Üstten asılı çelik kirişlerin tasarımında yanall burulmalı burkulma hesaba katılmalıdır. Üstten asılı kirişlerin bir özel türü de kren kirişleridir. İdeal yükleme ve sınır koşulları altındaki üstten asılı kirişlerin yanall burkulması, geçmişte klasik matematiksel prosedürler kullanılarak incelenmiştir. Bu tez, sonlu elemanlar metodunu kullanarak üstten asılı kirişler hakkında daha detaylı bir araştırma sunmayı amaçlamaktadır. Farklı yükleme ve sınır koşulları daha detaylı bir şekilde incelenmektedir. Kesit üzerinde yüklemenin yapıldığı noktanın ve desteklerin konumunun, burkulma kapasitesi üzerinde kayda değer etkileri olduğu görülmüştür. Farklı burulma ve burkulma özellikleri olan kirişler analiz edilmiştir. Tek ve çift çıkıntılı üstten asılı kirişler için kesit çarpılmasının burkulma kapasitesi üzerindeki etkileri incelenmiştir. Kesit çarpılması yüzünden ortaya çıkan kapasitedeki azalma miktarı nümerik olarak saptanmıştır. Analiz sonuçlarına dayanarak, üstten asılı kirişlerin yanall burkulması için basit tasarım önerileri oluşturulmuş ve bu tezin içerisinde sunulmuştur.

Anahtar Kelimeler: Yanall Burulmalı Burkulma, Üstten Asılı Kirişler, Kren Kirişleri

ACKNOWLEDGMENTS

The author wishes to express his deepest gratitude to his supervisor Assoc. Prof. Dr. Cem Topkaya for his guidance, advice, criticism, encouragements and insight throughout the research.

The author would also like to thank to committee members for their suggestions and comments.

TABLE OF CONTENTS

PLAGIARISM.....	iii
ABSTRACT.....	iv
ÖZ.....	v
ACKNOWLEDGMENTS.....	vi
TABLE OF CONTENTS.....	vii
CHAPTER	
1. INTRODUCTION.....	1
1.1 Background.....	1
1.2 Literature Survey.....	5
1.2.1 The Effective Length of Cantilevers as Governed by Lateral Buckling.....	5
1.2.2 Lateral Buckling of Overhanging Beams.....	5
1.2.3 Elastic Distortional Buckling of Overhanging Beams.....	5
1.2.4 Design of Cantilever Steel Beams: Refined Approach.....	6
1.2.5 Allowable Bending Stresses for Overhanging Monorails.....	6
1.3 Problem Statement.....	10
2. FINITE ELEMENT MODELING AND VERIFICATION.....	12
2.1 Finite Element Modeling Details.....	12
2.2 Verification of Finite Element Results.....	13
2.3 Effects of Loading and Boundary Conditions.....	16
3. ANALYSIS OF A SINGLE OVERHANGING MONORAIL.....	18
3.1 Instability under Different Boundary Conditions at Exterior Support.	18
3.2 Influence of Warping and Torsional Stiffness.....	22
3.3 Effects of Cross Section Distortion.....	31

3.4	A Caveat on Local Buckling.....	43
4.	ANALYSIS OF A DOUBLE OVERHANGING MONORAIL.....	46
4.1	Comparison of Single and Double Overhanging Beams.....	46
5.	SUMMARY AND CONCLUSIONS.....	51
5.1	Summary.....	51
5.2	Conclusions.....	51
	REFERENCES.....	53
APPENDIX		
A.	TABULAR DATA FOR GRAPHS.....	54

CHAPTER 1

INTRODUCTION

1.1 BACKGROUND

Beams are essential components of steel construction. A satisfactory design should ensure that the beam is stable and has enough strength and stiffness against the applied loads. For steel beams having an I-shaped cross section global buckling and local buckling are typical modes of instability. Global instability is in the form of lateral torsional buckling (LTB) of the beam as a whole while local instability could be in the form of web or flange buckling. Design codes present capacity equations for lateral torsional buckling of I-shaped members (AISC-LRFD, 2001). Local buckling is usually precluded by limiting the width-thickness ratio of the compression elements (web or flange).

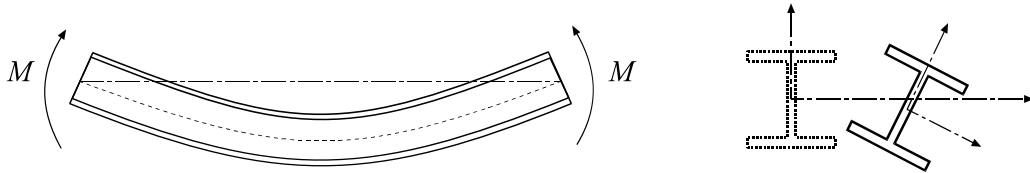


Fig. 1.1 – I-shaped beam in buckled configuration.

Lateral torsional buckling of I-beams is a complex phenomenon. If a simply supported beam is subjected to equal and opposite end moments as shown in Fig.1.1, the compression flange of the beam can move sideways when a certain value of applied moment is reached. In this undesirable behavior the tension flange tries to restrain the flange in compression and the resulting buckling mode is lateral-torsional indicating a lateral displacement together with a rotation of the cross section. Closed form solution (Eqn.1.1) of the critical buckling moment (M_{cr0}) has been developed (Timoshenko and Gere, 1961) and was adopted by many design codes (AISC-LRFD, 2001; TS-648, 1980) in different forms.

$$M_{cr0} = \frac{\pi}{L} \sqrt{EI_y GJ} \sqrt{1 + \frac{\pi^2 EC_w}{L^2 GJ}} \quad (1.1)$$

where: L : unbraced length
 E : modulus of elasticity
 I_y : minor axis moment of inertia
 G : shear modulus
 J : torsional constant
 C_w : warping constant

In the derivation of Eqn.1.1 it is assumed that the cross section is prevented from lateral movement and twist at the ends of the beam.

Due to the complexity of the problem it is difficult to come up with closed form solutions for cases with different loading and boundary conditions. Only a few closed form solutions exist for the lateral torsional buckling problem and mostly numerical methods are used for the solution of such problems.

For moment variations along the beam due to different loading conditions Eqn.1.1 needs to be modified to obtain the critical moment (M_{cr}). This is usually accomplished by multiplying the critical moment obtained from Eqn.1.1 by a moment gradient factor, C_b .

$$M_{cr} = C_b \times M_{cr0} \quad (1.2)$$

C_b is a modification factor for non-uniform bending moment variation along the laterally unsupported beam segment and depends on the shape of the moment diagram between lateral braces. C_b is dimensionless and varies between 1.0 and about 2.3 for simply supported and continuous beams.

Moment gradient factors have been developed in the past and the ones presented by the AISC specifications (AISC-LRFD, 2001) are given as follows:

$$C_b = \frac{12.5M_{\max}}{2.5M_{\max} + 3M_A + 4M_B + 3M_C} \quad (1.3)$$

where, M_{\max} : absolute value of maximum moment along the span
 M_A, M_C : absolute value of quarter point moment values
 M_B : absolute value of moment at the centre of span

$$C_b = 1.75 + 1.05 \left(\frac{M_1}{M_2} \right) + 0.3 \left(\frac{M_1}{M_2} \right)^2 \leq 2.3 \quad (1.4)$$

where, M_1 and M_2 are end moments as seen in Fig.1.2.

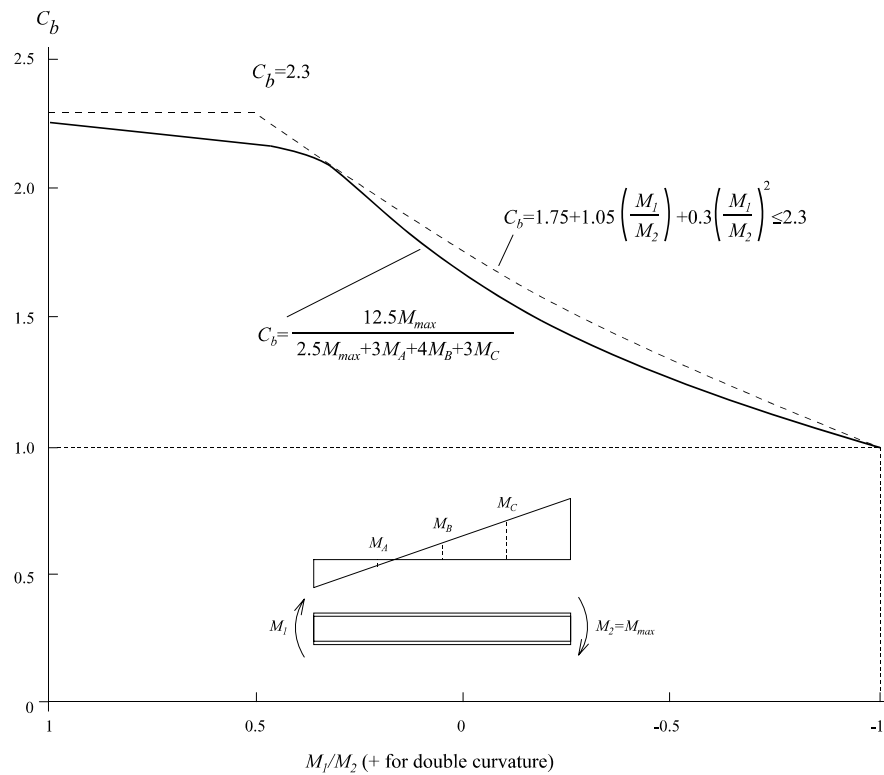


Fig. 1.2 – Comparison of C_b equations for linear variation of moment over laterally unbraced length.

Equation 1.3 is capable of representing the moment variation along the unbraced span better than Eqn.1.4 which is based on linear moment gradient. The support conditions assumed in the derivation of Eqn.1.1 are also valid for the cases with moment gradient.

Apart from simply supported and continuous beams, buckling of cantilevers was studied in the past (Timoshenko and Gere, 1961). Due to the differences in boundary conditions, cantilevers are treated differently than simply supported beams. In addition, overhanging beams which possess the characteristics of both cantilever and simply supported beams lend themselves to another special class of problems. In the case of an overhanging beam shown in Fig.1.3, there are either one or two cantilevering segments connected to a main span.

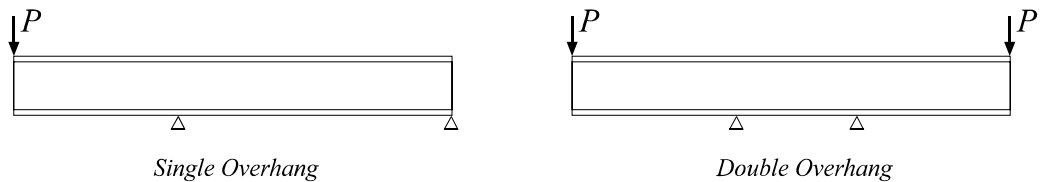


Fig. 1.3 – Generic view of a single overhanging beam and a double overhanging beam.

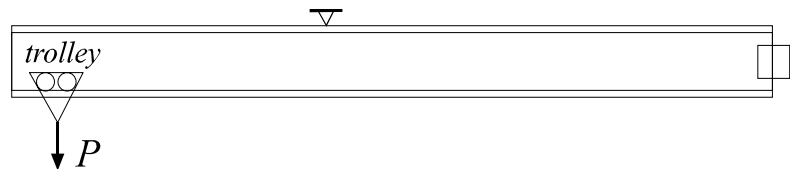


Fig. 1.4 – A typical crane trolley monorail.

One special type of overhanging beams is the crane trolley monorails shown in Fig.1.4. Overhanging monorails are quite frequently encountered in industrial structures. The monorail allows the movement of crane trolley through the entire span of the member. As in the general case of the overhanging beams monorail can have single or double overhangs. The design of crane trolley beams against global buckling is complex due to the nature of loading and boundary conditions. The next section presents a literature survey on buckling of overhanging beams in general and crane trolley monorails in particular.

1.2 LITERATURE SURVEY

The Effective Length of Cantilevers as Governed by Lateral Buckling (Nethercot, 1973):

In this study, Nethercot developed effective length factors for single and two span cantilevers. Finite element analysis was performed to study the behavior. Level of load application and the restraint conditions at the tip were varied. Effective length factors depending on the cross sectional properties and the loading/restraint conditions were presented. For two span cantilevers, it was shown that the vertical support condition at the root (interior support) had a negligible effect on stability.

Lateral Buckling of Overhanging Beams (Trahair, 1983):

In this paper, Trahair first presented some solutions for the buckling of built-in cantilevers subjected to end moment, point load and distributed load. Solutions for point loading was given for cases where the loading is at the top flange, shear centre and bottom flange. It was found that the bottom flange loading significantly increases the buckling capacity of cantilevers. Trahair showed that the built-in cantilever method for overhanging beams overestimates the resistance. Therefore, cantilevers with supports that allow warping were studied and capacity equations were presented. Based on the studies it was found that the results were virtually independent of the warping rigidity possessed by the beam. The recommendations presented for the cantilevers were used to develop an interaction buckling method for overhanging beams. The interaction buckling method takes into account the buckling of the main span and the overhanging segment individually. Finally, the effects of elastic torsional end restraints were studied and a family of curves was presented for overhanging beams having these kinds of restraints.

Elastic Distortional Buckling of Overhanging Beams (M.A. Bradford, 1994):

Bradford studied the elastic distortional buckling of overhanging beams. For this purpose a line type finite element was developed based on an earlier formulation by Bradford and Trahair (1981). This finite element is capable of representing the cross

sectional distortion during buckling. A generic simply supported beam with an overhang was studied where the ratio of main span to overhanging span was kept constant. In the analysis, top flange, shear centre and bottom flange loading was considered. Over the internal support the beam was either laterally supported or partially restrained like the beam on seats. The analysis results were presented in a non-dimensional form and the effects of cross section distortion on buckling capacity was displayed. The intent of the study was to shed light on one situation where distortion was found to be significant. No emphasis was given on the development of C_b factors.

Design of Cantilever Steel Beams: Refined Approach (Essa, Kennedy, 1994):

The main emphasis of this paper was to present effective length factors for doubly symmetric I-section cantilevers. Cantilevers were analyzed under different loading and boundary conditions using the finite element method. Based on the analysis results some recommendations on effective length of cantilevers were given. In addition, these researchers studied the instability of overhanging beams and crane trolley beams. For overhanging beams it was reported that the ratio of the cantilever span to backspan, loading and restraint conditions of both the cantilever end and the backspan are the factors that need to be considered. An interaction buckling model was proposed for the overhanging beams. Furthermore, a design procedure was given for estimating the elastic critical buckling moments of crane trolley beams. It was pointed out that the critical load positions are the tip of the overhang and the middle of the backspan; therefore, two separate checks are required for a proper design. In the development of design equations and the analysis, it was assumed that the beam is restrained against lateral deflection and twist at the support locations.

Allowable Bending Stresses for Overhanging Monorails (Tanner, 1985):

In this paper Tanner presented practical recommendations for design of overhanging monorails used for crane trolleys. A generic single overhanging monorail shown in Fig.1.5 was considered.

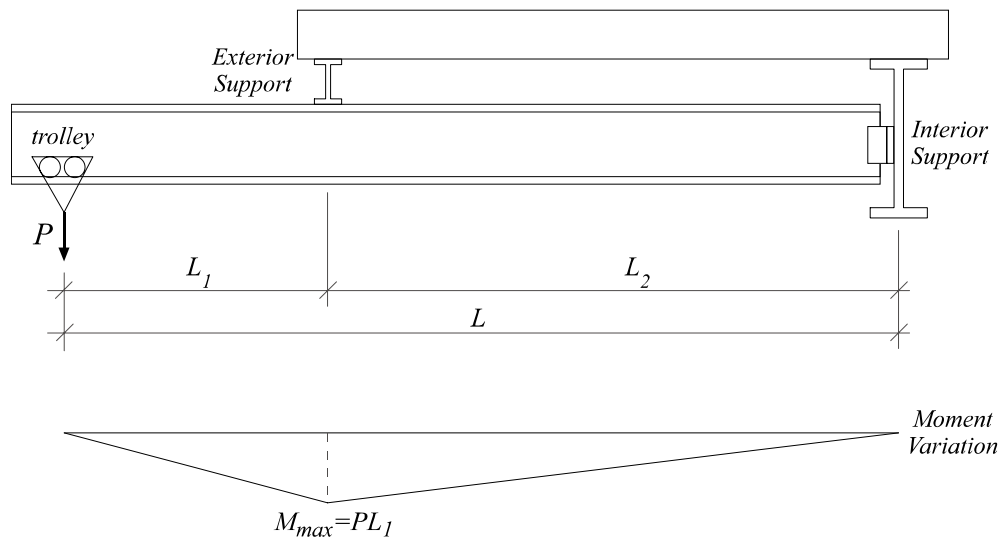


Fig. 1.5 – A typical single overhanging monorail.

As for the loading, the case where a point load acts at the end of the overhanging segment was considered. Due to this loading the entire length of the bottom flange is in compression. Therefore, the system can be analyzed as a simple beam with overhang. For a location to be considered as an LTB brace point, the cross section needs to be braced against twist or lateral displacement of the compression flange. For the case shown in Fig.1.5 the cross section is prevented from twisting at the interior support, therefore this location can be considered as a brace point. On the other hand, at the exterior support location, the displacement of the compression flange and twist are not restrained. In addition, it is not possible to restrain the end of the overhanging segment in order to have the lifting point clear of obstructions. The overhanging monorail is regarded as braced at the interior support only.

The system shown in Fig.1.5 was analyzed by Tanner using the classical mathematical procedures adopted for buckling of I-shaped beams. The beam was divided into two segments which comprise the main part and the overhanging part. For each part the differential equation that represents the equilibrium of the segment in the deformed configuration was written in terms of the torsional rotation. Later, the differential equations were solved using the Bessel functions and boundary conditions were applied to reduce the problem to a system of linear algebraic equations. The critical value of the

applied load was found by setting the determinant of the coefficient matrix of the system equal to zero.

Several assumptions were made during the solution of the problem which can be listed as follows:

- Material behaves linear elastic
- Transverse loads are applied through the shear centre of the cross section
- The cross section is doubly-symmetric I-shape
- Self weight of the beam is neglected
- The warping stiffness of the beam is negligible in comparison with the St.Venant torsional stiffness. Tanner focused on the solution for narrow flanged American standard shapes (S-shapes) which are commonly used for trolley beams. When the warping stiffness is neglected in Eqn.1.2 the critical buckling moment could be written as:

$$M_{cr} = \frac{C_b \pi}{L} \sqrt{EI_y GJ} \quad (1.5)$$

By using the procedure explained above, Tanner obtained a set of C_b values as a function of the non-dimensional parameter k which is defined as the ratio of the overhanging segment to the total beam length ($k=L_1/L$). The proposed C_b values based on the analyses were as follows:

Table 1.1 – The variation of C_b with changing k value

$k=L_1/L$	0	0.1	0.2	0.3	0.4	0.5	0.6	0.7	0.8	0.9	1.0
C_b	0.67	0.70	0.73	0.76	0.80	0.84	0.90	0.96	1.05	1.15	1.28

For simply supported and continuous beams laterally supported at the ends it is conservative to assume a C_b value equal to 1.0 for cases with moment gradients. The solutions given by Tanner showed that C_b values lower than 1.0 should be expected for overhanging beams when the total length of the beam (L) is used in Eqn.1.5. This point

was one of the most important outcomes of the study. In addition, the results presented in Table 1.1 seemed paradoxical because of the fact that lower critical moments occur for monorails with shorter relative overhangs. The physical reason behind this observation was explained by Tanner considering the two extreme cases.

For $k=1$;

In this case the system can be viewed as a cantilever under the action of a point load as depicted in Fig.1.6.

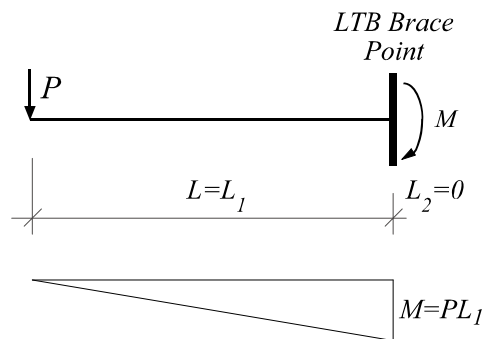


Fig. 1.6 – Theoretical solution for $k=1$

For a cantilever with fixed end braced and free end unbraced, the theoretical value of the C_b factor is $4.013/\pi=1.28$ (Timoshenko and Gere, 1961). Findings of Tanner are conformable with the theoretical derivations.

For $k=0$;

In this case the system can be viewed as a simply supported beam under the action of an end moment as shown in Fig.1.7.

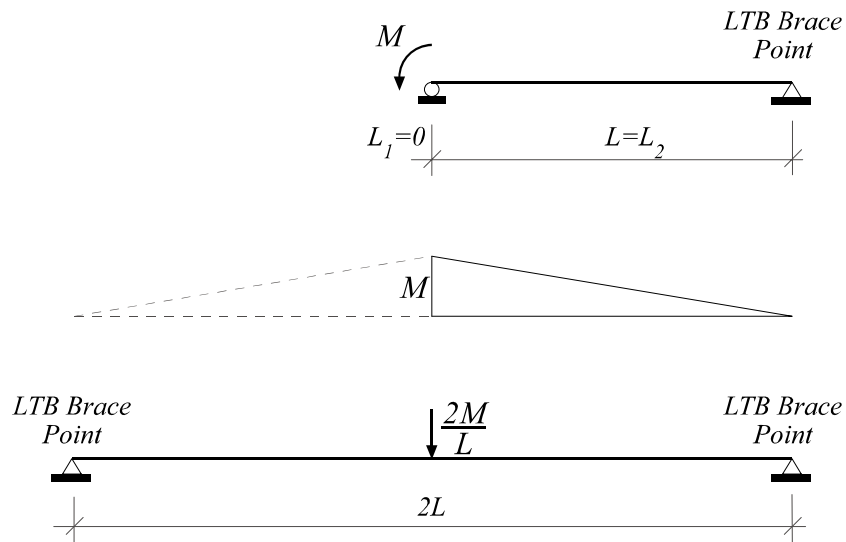


Fig. 1.7 – Theoretical solution for $k=0$

The simply supported beam has a brace point at one end and the other end is free to twist and displace laterally. By investigating the moment diagram and boundary conditions this system can be converted to an equivalent system having a length of $2L$ under the action of a load $2M/L$. The theoretical solution for a beam under the action of a point load at the midspan gives a C_b value of $17.2/4\pi = 1.37$ (Timoshenko and Gere, 1961). For the case of a simply supported beam with end moment this converts simply a C_b value of $1.37/2 = 0.685$ which is also conformable with the findings of Tanner.

According to these observations it was explained that case where $k=0$ produces an unfavorable moment diagram compared to the case where $k=1$. For the case $k=1$, the maximum disturbing moment occurs at the brace point while for the case where $k=0$ the maximum moment occurs at the unbraced location. Therefore, the critical moment is less for beams with shorter overhanging portion.

1.3 PROBLEM STATEMENT

As presented before little has been done to quantify the buckling capacity of overhanging monorails. The design recommendations presented by Tanner (1985) are based on a theoretical solution which only encompasses ideal support conditions. In

reality the boundary conditions at the exterior support can vary significantly. In addition, bottom flange loading is more commonly encountered in practice compared to the shear centre loading. This thesis aims to present a rigorous numerical study on buckling of overhanging monorails used for crane trolleys.

Due to the complexity of the problem, the finite element method was adopted as a numerical analysis procedure. Using the finite element method, buckling of overhanging monorails under different load and boundary conditions has been studied. A parametric type of study has been undertaken to understand the important parameters that influence the instability response.

In chapter two, the details of the finite element methodology are presented and the findings of Tanner (1985) and the numerical analyses are compared. In chapter three, a monorail with a single overhanging segment is analyzed under different boundary conditions. Different section dimensions are considered to investigate the effect of cross section distortion. In chapter four, the analysis results presented in chapter three are extended to monorails with double overhangs. Finally, in chapter five, the conclusions are given along with the design recommendations.

CHAPTER 2

FINITE ELEMENT MODELING AND VERIFICATION

2.1 FINITE ELEMENT MODELING DETAILS

In this thesis the buckling of overhanging monorails was studied in detail using the finite element method. As mentioned before due to the complexity of loading and boundary conditions, it is difficult to come up with closed form solutions. Rather numerical methods are employed to investigate the instability behavior. Finite element analysis could be conducted using either beam or shell elements for this problem. Most of the beam elements developed can be used for ideal boundary conditions. On the other hand if complex boundary conditions exist such as presence of stiffeners; a global three dimensional modeling with shell elements is preferred.

Throughout this study, overhanging monorails were modeled using shell elements with 8 nodes. Numerical analysis were performed using a commercially available software ANSYS (ANSYS, 2003). The cross section of the beam was modeled using the centerline distances between the plates and the curved portions were not modeled. The beam web and flanges were usually divided into four shell elements. Depending on the point of application, the load was placed at the top flange, the bottom flange or at the shear centre of the cross section. Different boundary conditions that will be explained later in detail were used during the analysis. A representative finite element mesh is given in Fig.2.1.

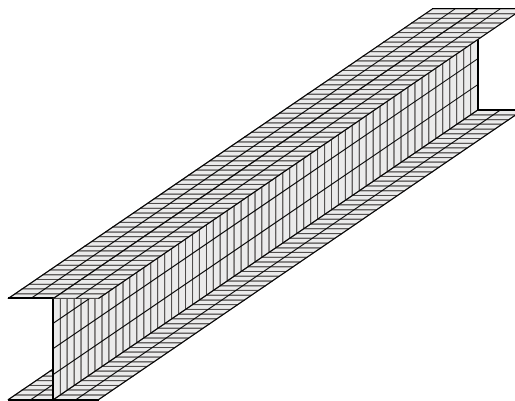


Fig. 2.1 – Finite element model of the beam.

For each overhanging beam with certain loading and boundary conditions a finite element mesh has been prepared. Later, a linear bifurcation buckling analysis has been conducted to find the lowest eigenvalue of the system. The eigenvalue obtained from the numerical analysis was converted to a critical buckling moment and a C_b value for that particular analysis.

2.2 VERIFICATION OF FINITE ELEMENT RESULTS

A generic overhanging monorail was analyzed in order to verify the findings of finite element analysis. For this purpose, a narrow flange American S-shape (S12x40.8) profile was chosen. The properties of the section are given in Fig.2.2.

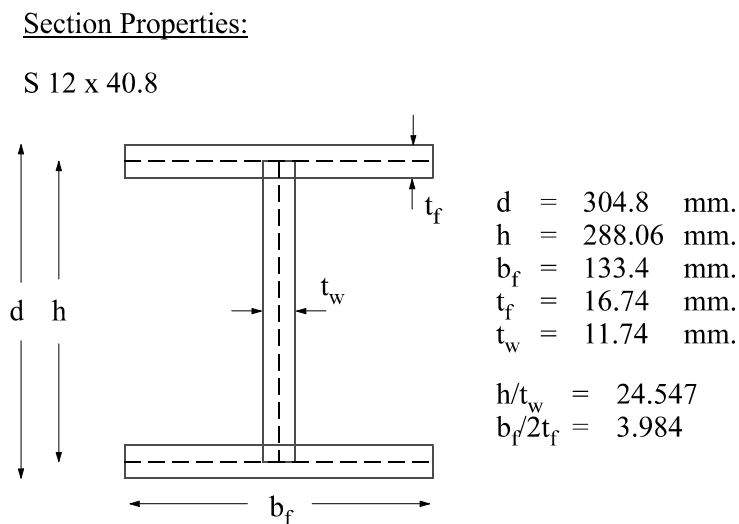


Fig. 2.2 – Section properties of an S12x40.8 American S-shape.

The total length of the beam was taken as 6m. The location of the exterior support was changed to have a k value that varies between 0.1 and 0.9. As mentioned before, the recommended C_b values by Tanner are based on an analysis where the loading is at the shear centre. In addition, the beam is supported vertically from the shear centre at the exterior support location. In order to be able to make comparisons with Tanner's (1985) findings, same boundary conditions were applied to the finite element model in this verification work. The vertical and lateral displacements of the nodes that lie on the

line of the web at the interior support were prevented from movement to provide a lateral brace at that location. The summary of the loading and boundary conditions are given in Fig.2.3.

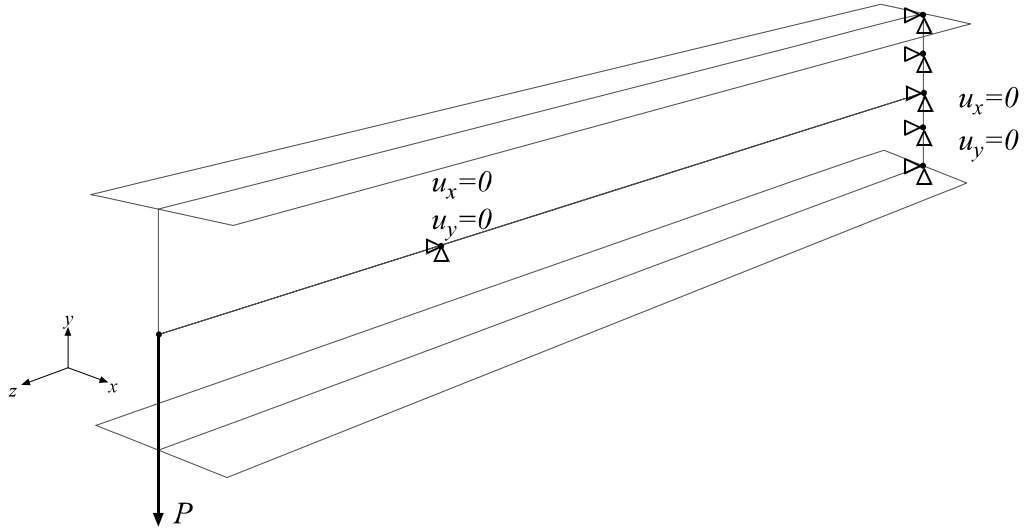


Fig. 2.3 – Boundary conditions and loading for the beam.

The eigenvalue of each analysis case has been converted to a buckling moment. Later this buckling moment has been converted to a C_b value by normalizing with the critical moment obtained from the case with equal and opposite end moments. In this conversion, two C_b values were found for each case. For the first one, the warping stiffness was included in the critical moment equation while for the second one the warping stiffness was neglected. In other words, The M_{cr0} expressions used for the normalization are as follows:

$$M_{cr0}(w-inc) = \frac{\pi}{L} \sqrt{\left(\frac{\pi E}{L}\right)^2 C_w I_y + EI_y GJ} \quad (2.1)$$

$$M_{cr0}(w-exc) = \frac{\pi}{L} \sqrt{EI_y GJ} \quad (2.2)$$

It should be noted that the Tanner's (1985) solution excluded the warping stiffness term. For the S12x40.8 section having a length of 6m, the M_{cr0} values are 136.3 kN-m and 125.8 kN-m for the warping included and excluded, respectively.

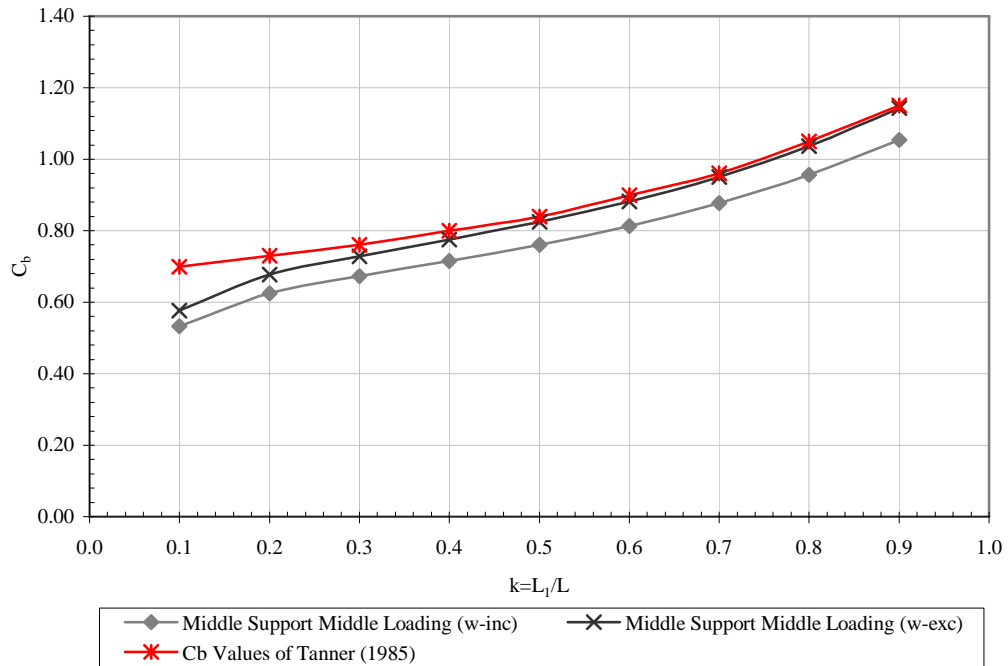


Fig. 2.4 – Comparison chart of Tanner's findings (1985) and analysis results.

The variation of C_b as a function of k is given in Fig.2.4. In this figure, the C_b values obtained by both normalizing with respect to Eqn. 2.1 and 2.2 are given. In addition, the Tanner's (1985) solution is provided for comparison purposes. As can be seen from Fig. 2.4 finite element analysis provides acceptable capacity predictions when compared with the closed form solutions. For low k values, finite element analysis captured local effects; therefore, C_b values for this range are lower than the ones recommended by Tanner (1985). As expected the C_b values should be lowered if the warping stiffness terms need to be included in the M_{cr0} expression. Next section will present a detailed analysis of the effect of boundary and loading conditions.

2.3 EFFECTS OF LOADING AND BOUNDARY CONDITIONS

The solution presented by Tanner (1985) is for the ideal case where the loading and boundary condition at the exterior support is applied at the shear centre. On the other hand, in reality, the loading is usually applied at the bottom flange and vertical exterior support is applied at the top flange. In order to enhance the findings of Tanner (1985), a detailed investigation on loading and boundary conditions has been conducted. The same S12x40.8 beam has been analyzed under the following four loading and boundary conditions.

1. The exterior support at the shear center and loading at the shear center (Middle support middle loading - MSML)
2. The exterior support at the shear center and loading at the bottom flange (Middle support bottom loading - MSBL)
3. The exterior support at the top flange and loading at the shear center (Top support middle loading - TSML)
4. The exterior support at the top flange and loading at the bottom flange (Top support bottom loading - TSBL)

Case 1 (MSML) is the same as the one of Tanner's (1985) system whereas Case 4 (TSBL) is a commonly encountered condition. The C_b values were derived from normalizing the buckling moments with the critical moments (Eqn.2.1) obtained considering the warping stiffness term. Fig.2.5 presents the variation of C_b values as a function of k for the four cases.

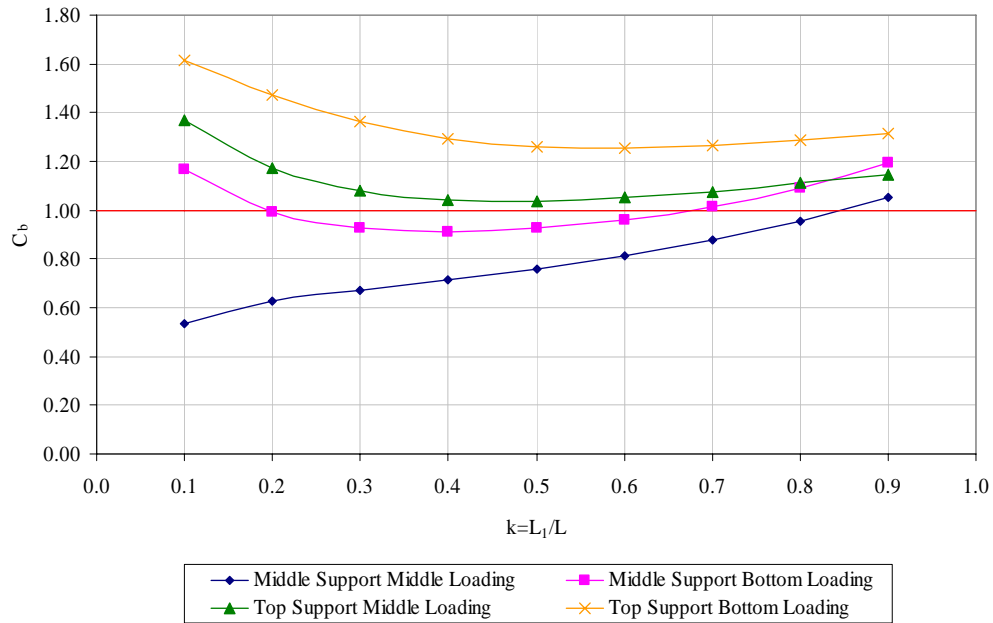


Fig. 2.5 – Comparison chart of Tanner’s findings (1985) and analysis results for different loading and boundary conditions

Examination of Fig.2.5 revealed that C_b values change drastically with the changes in boundary conditions. It is observed that the C_b values tend to increase as the loading is applied at the bottom flange rather than the shear centre. The same conclusion is valid when the top flange support is applied rather than the support at shear centre. For most commonly used case among all (TSBL) the C_b values are all greater than one and its variation with k is different than the ones for other cases. These findings clearly show that there is need for a more rigorous numerical analysis on overhanging monorails. The following chapter will present in detail the findings of a parametric investigation conducted to understand the buckling behavior of overhanging monorail systems.

CHAPTER 3

ANALYSIS OF A SINGLE OVERHANGING MONORAIL

3.1 INSTABILITY UNDER DIFFERENT BOUNDARY CONDITIONS AT EXTERIOR SUPPORT

As shown in the previous chapter, the critical buckling loads for overhanging monorails are greatly influenced by loading and boundary conditions. The design recommendations given by Tanner (1985) are based on solutions using shear centre loading and idealized boundary conditions. Based on a more refined analysis that was presented in Chapter 2, it was observed that C_b values greater than unity could be used for more realistic cases. In the case that was analyzed in Chapter 2, it was assumed that the exterior support was placed at the top flange. In this idealized boundary condition, the vertical moment of the point where the top flange and web meets was prevented. This kind of a boundary condition does not prevent the twist of the section. In reality, due to the attachment details, certain degree of twist restraint is present at the exterior support location. A resistance against twist at this support may significantly increase the buckling capacity. In this chapter, more detailed analyses are performed to investigate the effects of different boundary conditions that may be present at the exterior support location.

For this purpose, 7 different boundary conditions were considered in the analyses. The boundary conditions that were considered are given in Fig. 3.1.

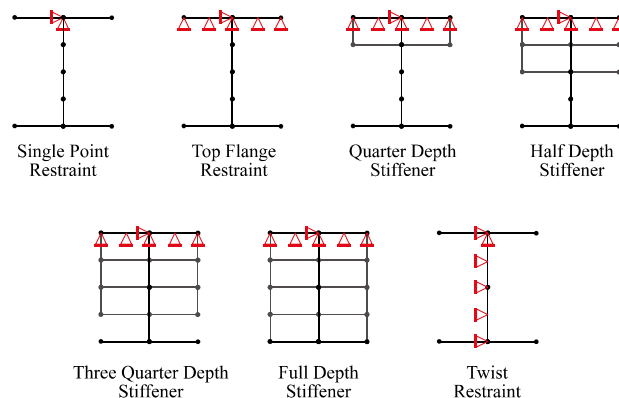


Fig. 3.1 – Boundary conditions at the exterior support.

The details of the boundary conditions are as follows:

1. **Single point restraint (SPR):** The top flange – web junction is restrained against vertical translation and the section is free to rotate.
2. **Top flange restraint (TFR):** The vertical translation of the flange is restrained. There is certain degree of restraint against twist which is based on the web flexibility.
3. **Quarter depth stiffener (QDS):** Same boundary conditions as the top flange restraint (TFR). In addition, a pair of stiffeners is placed on both sides of the web. The stiffeners have a width equal to half the flange width. Stiffeners are extended to $\frac{1}{4}$ depth of the beam from the top. The stiffener thickness is equal to the thickness of the top flange.
4. **Half depth stiffener (HDS):** Same as case 3 except that the stiffeners are extended to the half depth of the beam.
5. **Three quarter depth stiffener (TQDS):** Same as case 3 except that the stiffeners are extended to the $\frac{3}{4}$ depth of the beam.
6. **Full depth stiffener (FDS):** Same as case 3 except that the stiffeners are extended to the full depth of the beam.
7. **Twist restraint (TR):** The vertical movement of the top flange and the horizontal out of plane movement of the web are prevented. The cross section can not twist or distort at the exterior support location.

In order to investigate the effects of these 7 boundary conditions, an S12x40.8 beam with 6m length was considered. The exterior support location was changed to have k values between 0.1 and 0.9. A point load was placed at the tip of the overhanging portion at the junction of web and bottom flange. Twist was restrained at the interior support. For each combination of boundary condition and support location an eigenvalue buckling analysis was performed. The eigenvalues were documented and then used to calculate the critical buckling moment at the exterior support location. These critical moment values were normalized by M_{cr0} (*w-inc*) which is previously given in Eqn. 2.1. The variation of C_b value as a function of k for different boundary conditions is given in Fig. 3.2. Representative buckled shapes for the 7 cases ($k=0.5$) are given in Fig. 3.3.

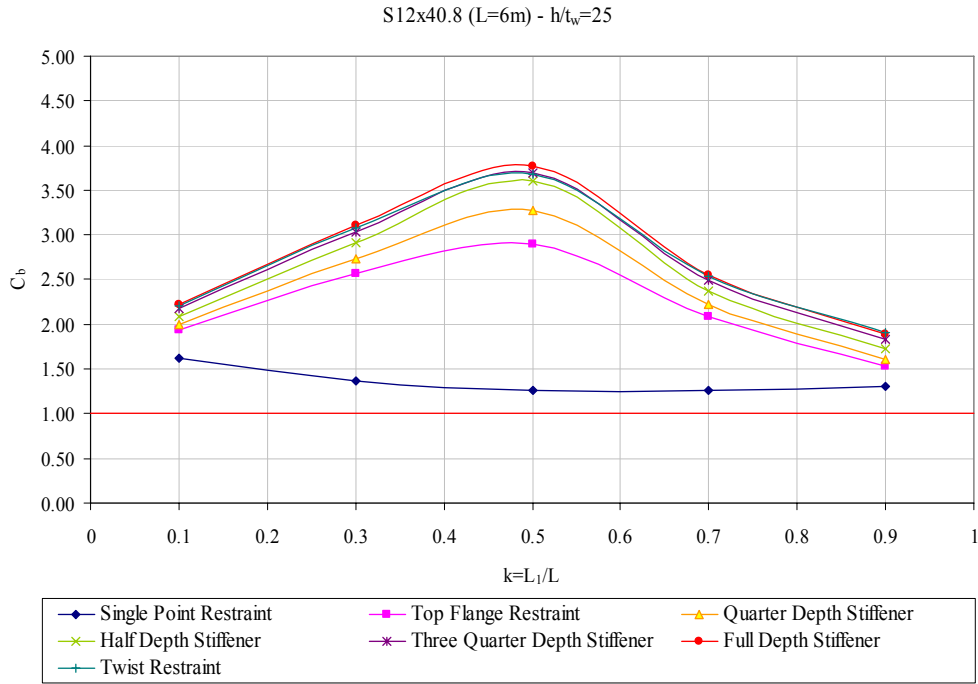


Fig. 3.2 – Comparison of different boundary conditions for S12x40.8 beam with 6m length.

Examination of Fig 3.2 reveals that boundary conditions have significant effects on the C_b values. For the case where there is single point restraint (SPR), the C_b values stayed below 2.0 and there was a decrease with the increase in the k value. Even in this case, all C_b values were higher than unity. For the single point restraint (SPR) the cross section is allowed to twist and this is clearly observed from the buckled shapes (Fig. 3.3a). On the other hand, providing vertical restraints to the top flange greatly increases the buckling capacity. For the top flange restraint (TFR) case, the variation of C_b with k values is different when compared with the single point restraint (SPR) case. For the TFR case, C_b values exhibit a parabolic variation with k values. When the movement of the top flange is restrained, the cross section is not fully allowed to twist. The degree of twist and the amount of lateral movement of the bottom flange is influenced by the flexibility of the beam web. For the S12x40.8 beam analyzed, it is observed that C_b values could reach to 3.0 (for $k=0.5$) by restraining the top flange movement. This observation suggests that the web stiffness could be relied on in increasing the buckling capacity.

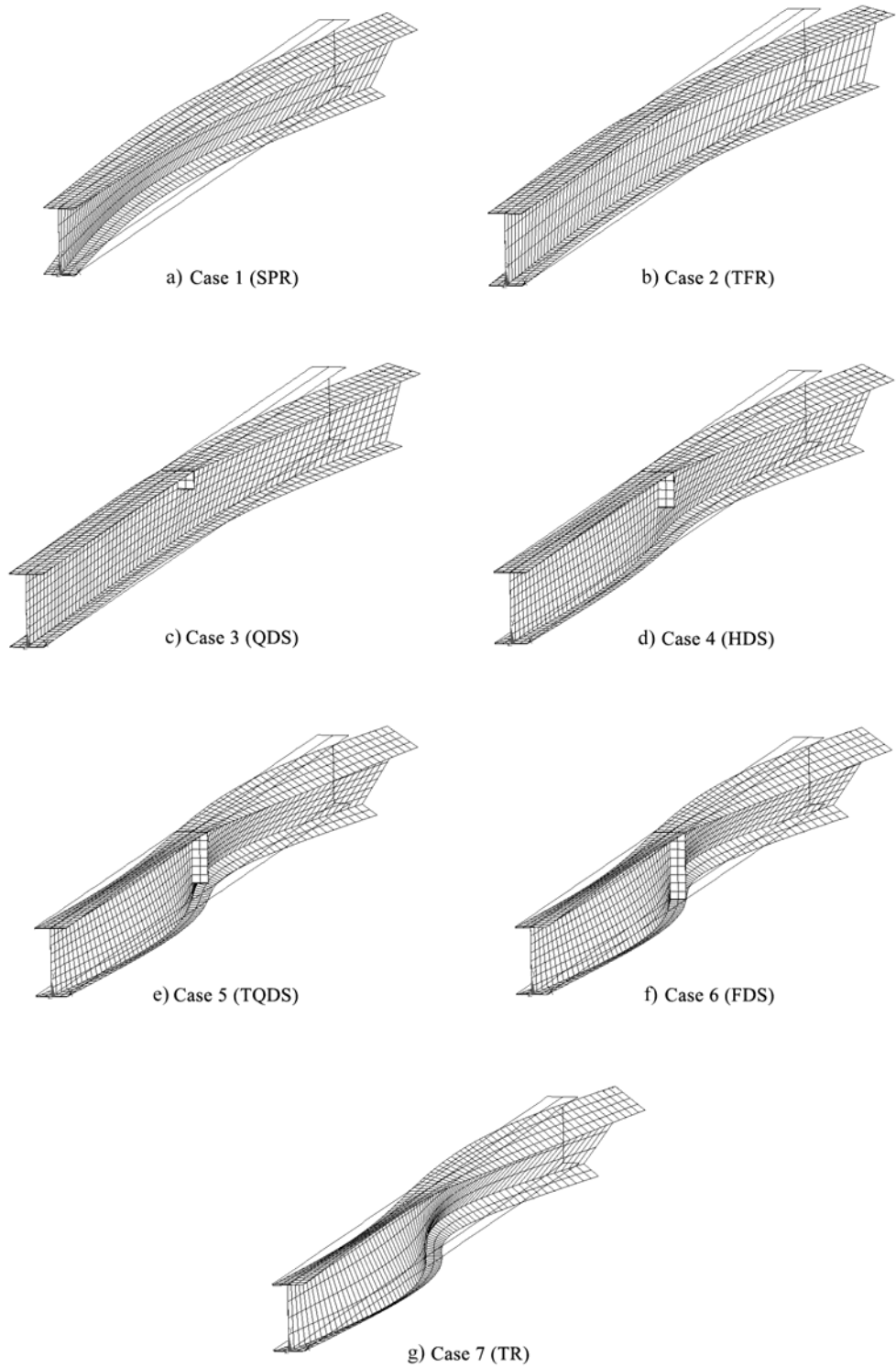


Fig. 3.3 – Buckled shapes for different boundary conditions for $k=0.5$.

As the depth of the stiffener is increased the stiffness of the web against distortion is increased. Any increase in the stiffness of the web is expected to result in an increase in the buckling capacity. This fact is clearly observed in Fig 3.2. Placing a $\frac{1}{4}$ depth stiffener increases the C_b values for the k range of interest. For the analyzed beam, it seems that placing $\frac{1}{2}$, $\frac{3}{4}$ and full depth stiffeners virtually give the same capacity. As the depth of the stiffener reaches to the depth of the beam, the results for C_b approach to the result of the twist restraint case. When compared with Tanner's (1985) recommendations, the C_b values could be increased by 6-7 fold by applying a more rigorous analysis.

The results presented in Fig 3.2 could be converted into design recommendations. However, the applicability of these findings to different cross sections and beam geometries needs further investigation. In the following sections, beams with different geometric properties will be explored to find out the ranges of applicability.

3.2 INFLUENCE OF WARPING AND TORSIONAL STIFFNESS

Both warping and torsional stiffness possessed by the beam contributes to the lateral buckling capacity. As explained before, Tanner (1985) excluded the warping stiffness term in calculating the critical buckling moment. This assumption is valid for narrow flanged S-shapes. However, for other sections neglecting the warping stiffness might be an overly conservative assumption.

If Eqn. 1.1 for critical buckling moment is examined, it could be seen that the warping stiffness contributes to the term in the square root. Usually the ratio of the warping stiffness to torsional stiffness could be expressed as a non-dimensional factor, herein called as α , where

$$\alpha = \frac{\pi^2 EC_w}{L^2 GJ} \quad (3.1)$$

The α factor is compared against unity to decide on the respective contribution of the warping stiffness term. For beams having an α value much less than 1.0 the warping stiffness could be neglected. For the 6m long S12x40.8 beam, the α factor is equal to

0.17. This indicates that neglecting the warping stiffness results in 8 percent less capacity than the actual.

In order to understand the effects of the warping contribution term similar analysis were performed using three other cases. In the first case, a beam length of 3 meters was considered for the same S12x40.8 section. A shorter length results in an α factor of 0.70. For the two other cases, beams having different cross sectional properties but 6 meter length were considered. The cross sectional properties of the sections considered (SEC1, SEC2) are given in Fig 3.4. The resulting α factors for SEC1 and SEC2 are 1.04 and 2.09, respectively. The S12x40.8 and SEC1&2 have h/t_w values close to 25 and their $b_f/2t_f$ values varied between 4 and 6.67.

Section Properties:

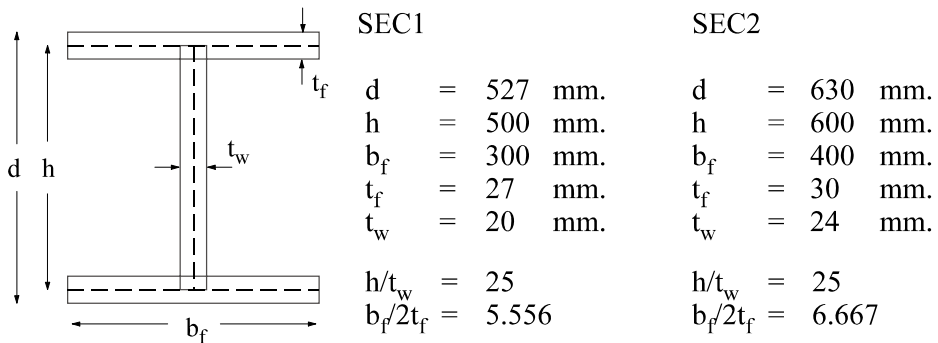


Fig. 3.4 – Cross sectional properties of SEC1 and SEC2.

For the three cases mentioned above, analyses were conducted by considering 7 different exterior support conditions and k values ranging from 0.1 to 0.9. In Figs. 3.5 to 3.7, for these three cases, C_b values for 7 different boundary conditions were displayed.

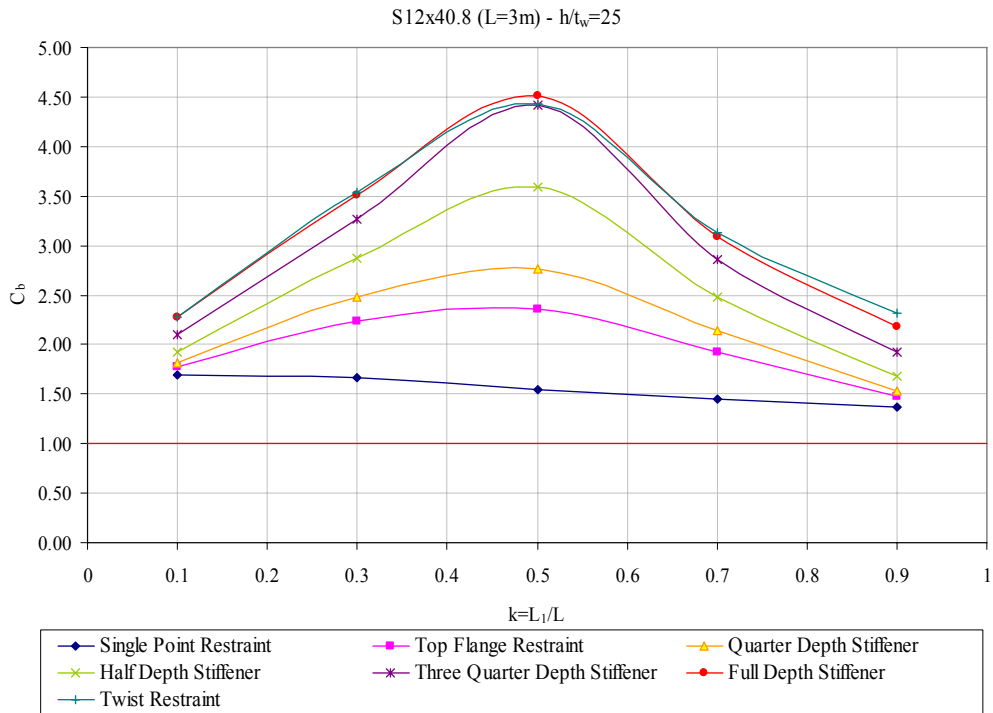


Fig. 3.5 – Comparison of different boundary conditions for S12x40.8 beam with 3m length.

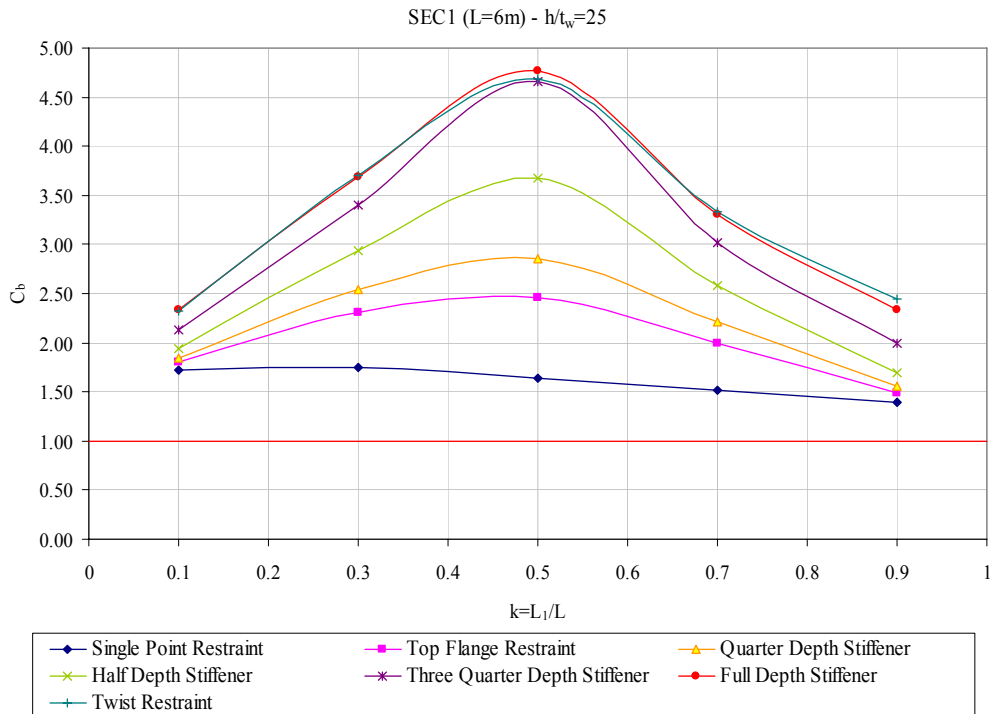


Fig. 3.6 – Comparison of different boundary conditions for SEC1 beam with 6m length.

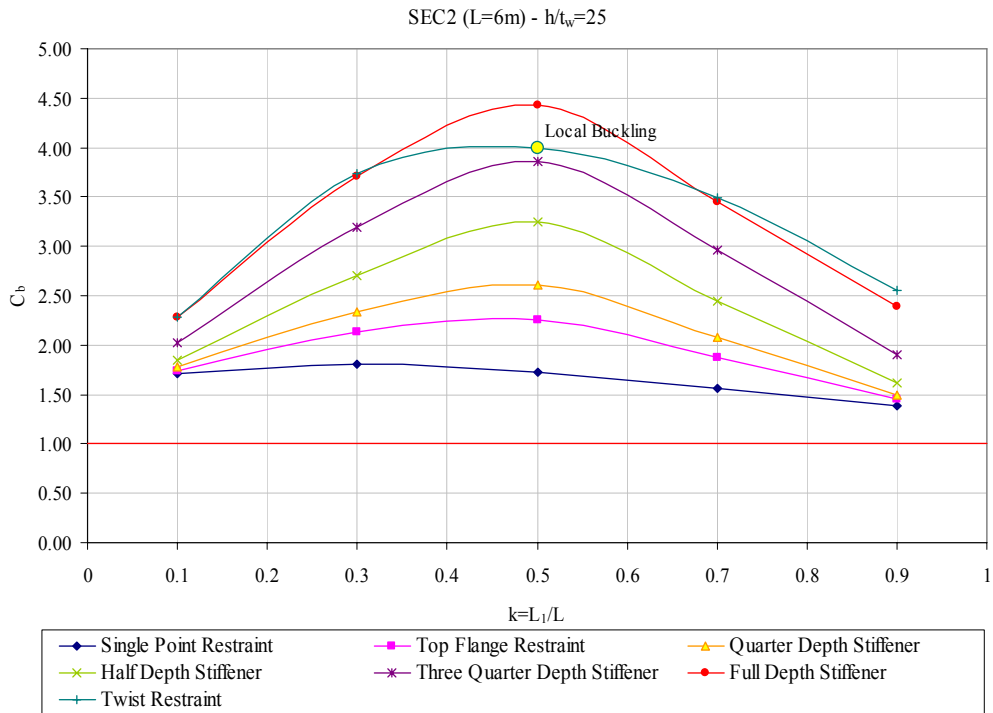


Fig. 3.7 – Comparison of different boundary conditions for SEC2 beam with 6m length.

Also to observe the behavior of the contribution term α for these cases, the C_b values obtained for systems having different α values are compared in Figs. 3.8 to 3.14. In these figures the variation of C_b value as a function of k is presented for overhanging monorails having α values of 0.17, 0.70, 1.04 and 2.09.

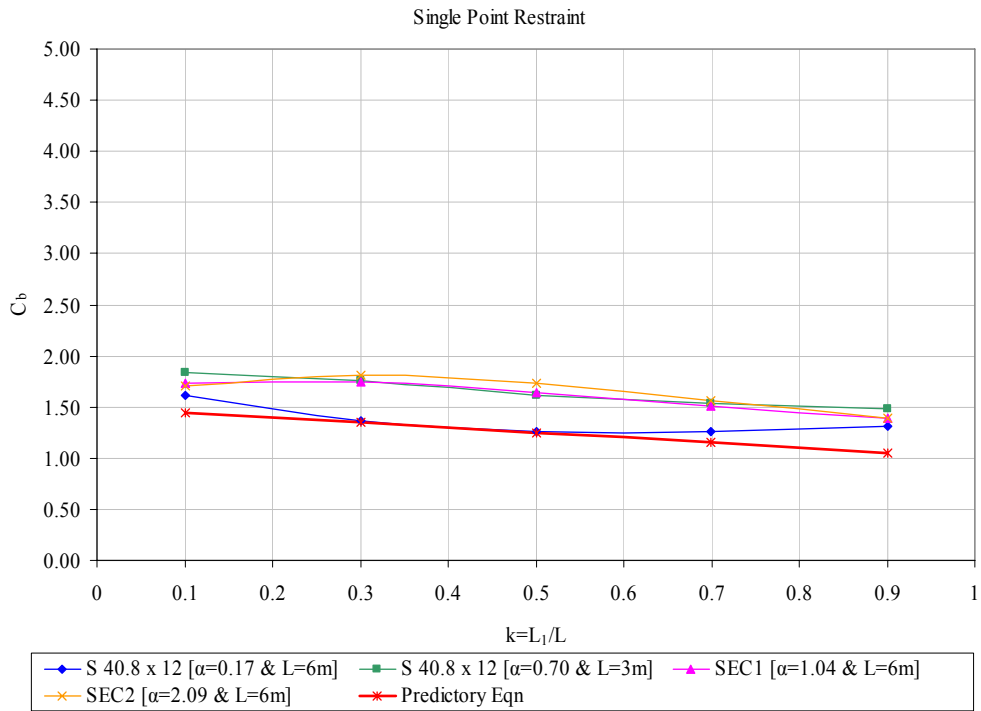


Fig. 3.8 – Comparison of different sections for single point restraint (SPR) case.

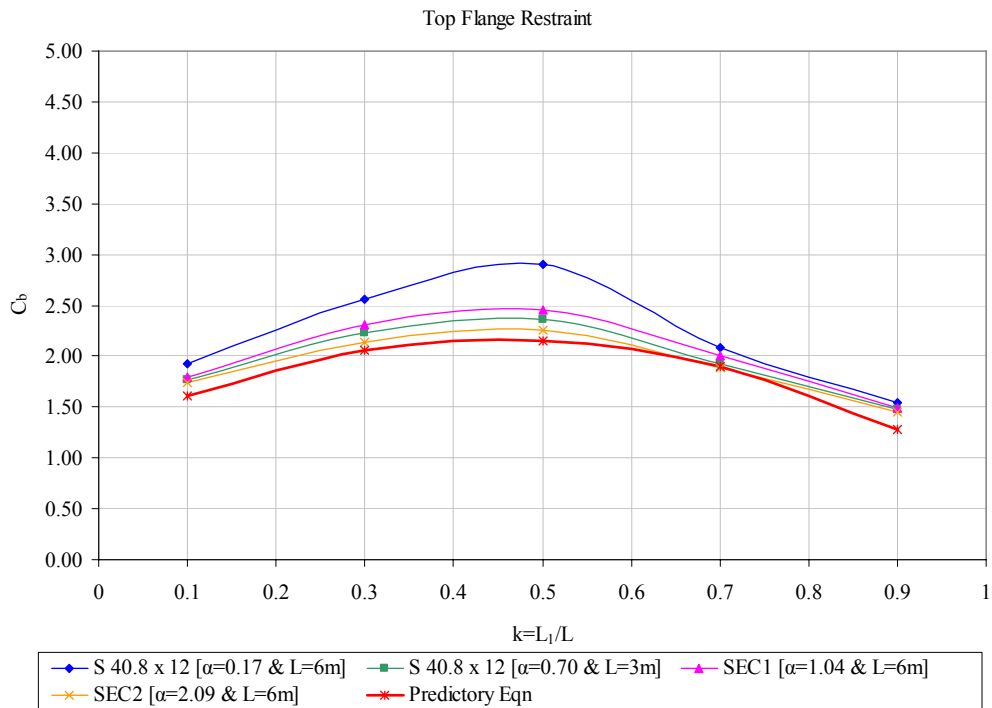


Fig. 3.9 – Comparison of different sections for top flange restraint (TFR) case.

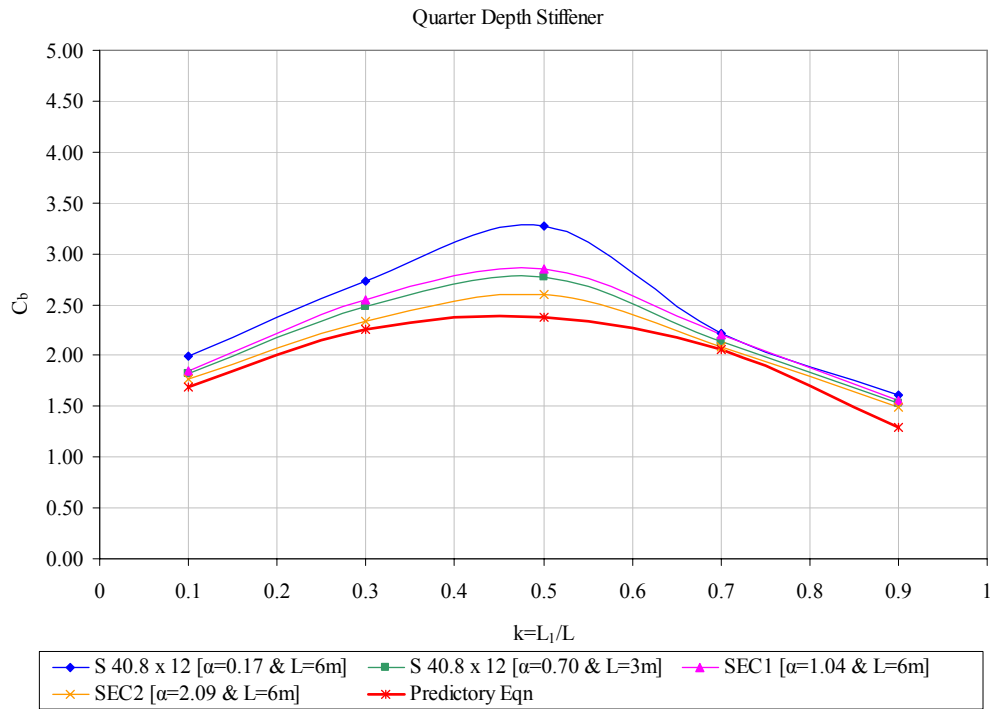


Fig. 3.10 – Comparison of different sections for quarter depth stiffener (QDS) case.

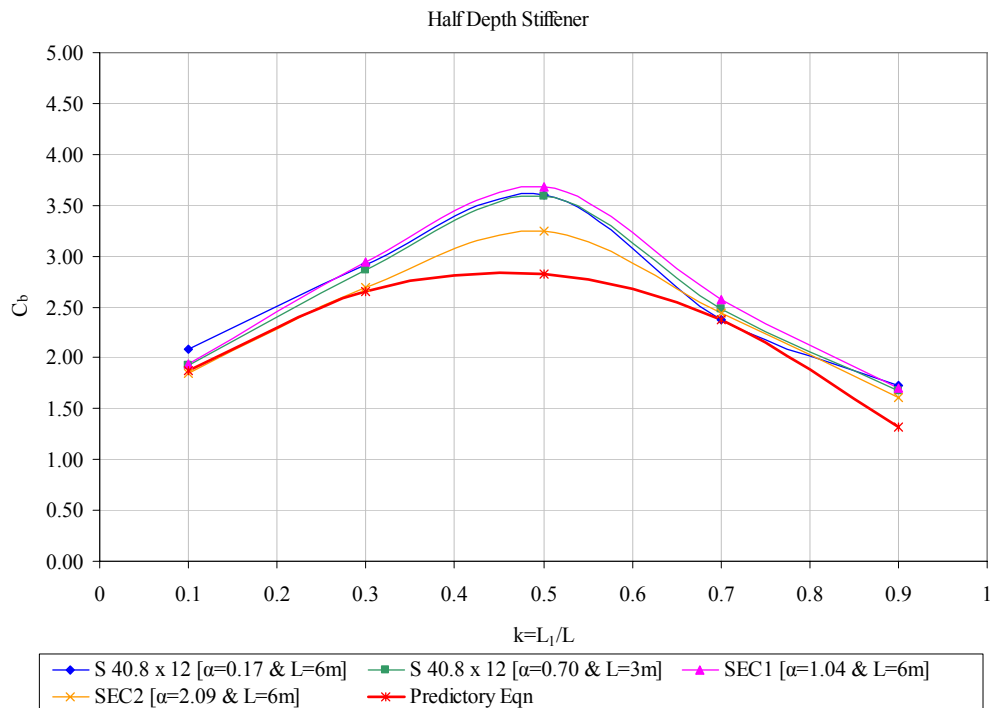


Fig. 3.11 – Comparison of different sections for half depth stiffener (HDS) case.

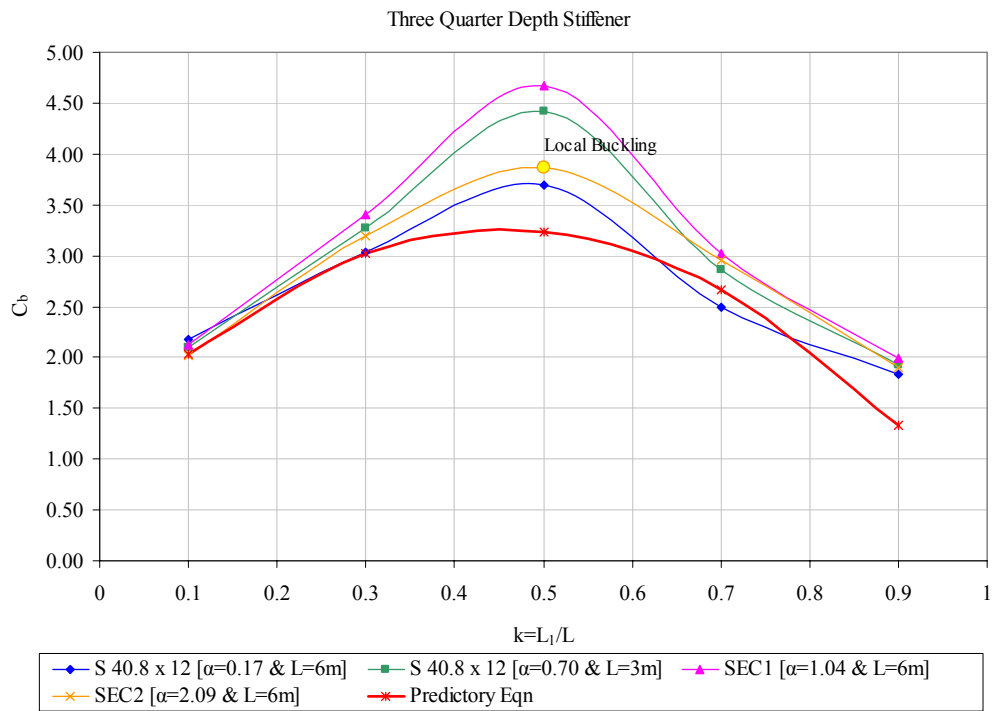


Fig. 3.12 – Comparison of different sections for three quarter depth stiffener (TQDS) case.

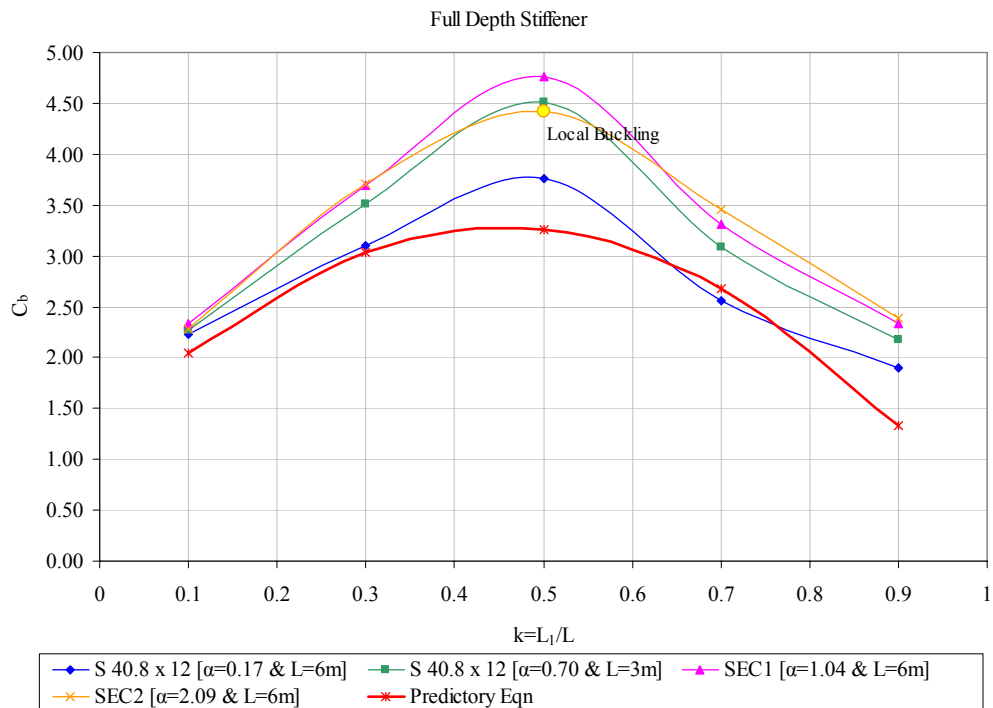


Fig. 3.13 – Comparison of different sections for full depth stiffener (FDS) case.

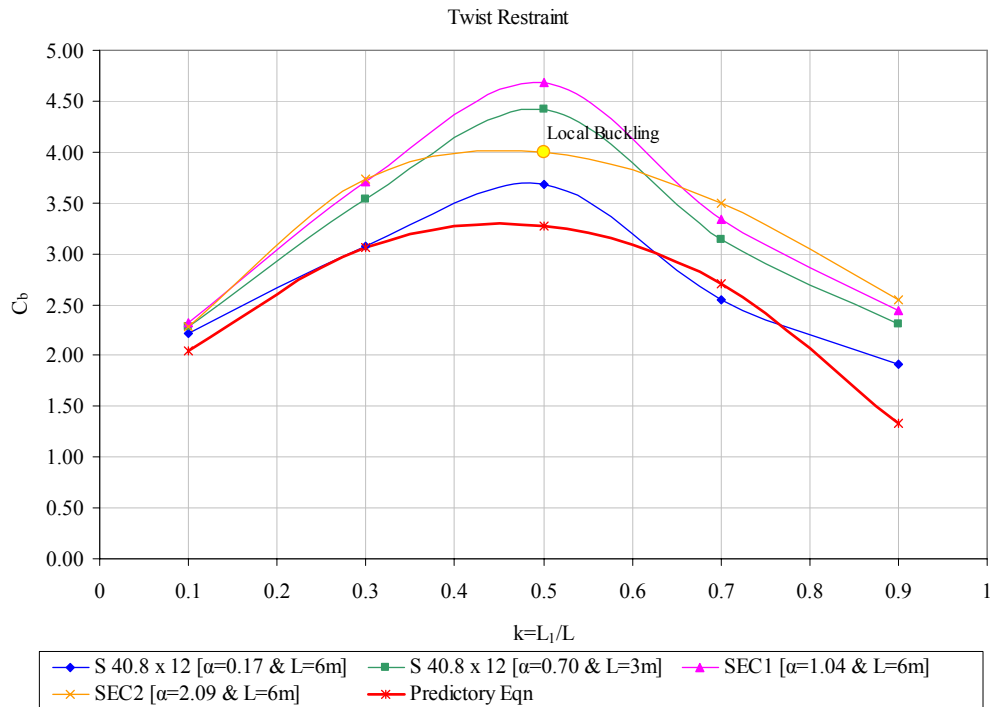


Fig. 3.14 – Comparison of different sections for twist restraint (TR) case.

When the comparison graphs are examined no definite conclusions could be drawn for the effect of warping stiffness. For all the boundary conditions the data points for sections for different α values fall within a narrow band. Response of various sections could be grouped into three depending on the boundary conditions. For the single point restraint (SPR) case, C_b values tend to increase with the increase in the α value. For the top flange restraint (TFR), quarter depth stiffener (QDS) and half depth stiffener (HDS) cases, the behavior is more erratic. Under these boundary conditions, the section having an α value of 0.17 produces the highest C_b values. The C_b value decreases as α value is increased. The section with an α value of 0.70 gives lower C_b values compared to the section with an α value of 1.04. This deviation from the general trend is inconclusive. However, it should be pointed out that the deviation occurs for the case where the beam length is 3m. If sections with the same beam length ($L=6m$) are considered, then it is observed that the C_b values tend to decrease with an increase in the α value. For the three quarter depth stiffener (TQDS), full depth stiffener (FDS) and twist restraint (TR) cases, C_b values tend to increase with an increase in the α value. When case of $k=0.5$ is considered, the section with an α value of 2.09 gives smaller C_b values when compared

to the section with an α value of 1.04. This is attributable to the local buckling effects observed during the examination of buckled shapes.

As mentioned before, most of the data points fall within a band. It is possible to develop design expressions for different boundary conditions and for sections having different warping stiffnesses. Development of such expressions will yield in complicated design equations. For practical purposes, conservative lower bound equations are developed in this thesis. First of all, due to the differences in the variation of C_b values, a separate expression is developed for the single point restraint (SPR) case. For this boundary condition, a linear variation with k could be assumed. Based on this assumption, the predictory lower bound equation developed is given as follows:

$$C_b = -0.5 k + 1.5 \quad (3.2)$$

The plot of the prediction equation is given in Fig. 3.8.

For all other boundary conditions, the response could be represented by a parabola. By using curve fitting and rounding off the coefficients, the following equation was developed for the 6 boundary conditions:

$$C_b = -1.1 \beta k^2 + \beta k + 1.25 \quad (3.3)$$

where β : Constant depending on the boundary condition (see Table 3.1)

Table 3.1 – β table for 6 boundary conditions.

	TFR	QDS	HDS	TQDS	FDS	TR
β	4	5	7	8.8	8.9	9

The plots of the predictions are also given in Figs 3.9 through 3.14.

It should be pointed out that the full depth stiffener and the twist restraint cases are actually impractical. These can not be implemented because of the trolley that is moving along the beam length. However these cases present the theoretical upper bounds on the capacity.

3.3 EFFECTS OF CROSS SECTION DISTORTION

Analysis results presented so far showed that the boundary conditions at the exterior support location have significant effects on the buckling capacity. If the vertical movement of the top flange is restrained at the exterior support then one has to rely on the bending stiffness of the web. In deriving the classical lateral torsional buckling moment equation (Eqn. 1.1) it is assumed that the cross section goes through a rigid body motion. However, in reality if the web is slender, significant amount of cross section distortion can occur and as a result, the buckling capacity may be reduced. Typical cross section distortion is depicted in Fig. 3.15.

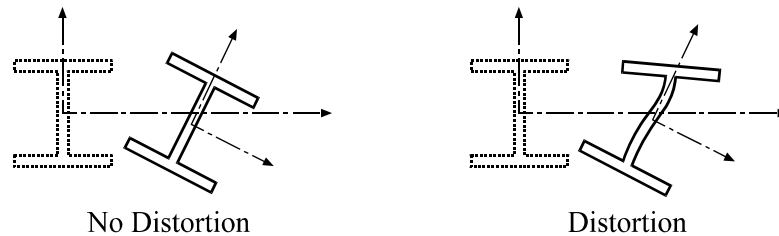


Fig. 3.15 – Pictorial view of cross section distortion.

The effects of cross section distortion on lateral buckling capacity have been studied in the past. (Bradford and Trahair, 1981; Bradford, 1992; Pi and Trahair, 2000) For the problem at hand, the effects of distortion at the exterior support need to be studied in order to extend the recommendations to beams having slender webs. For this purpose, the same S12x40.8 beam with 6m length was considered. The analyzed beam has an h/t_w value of 25 and an α value of 0.17. The web thickness of the beam was reduced to get sections with h/t_w values of 40, 60 and 80. For this cross section and beam length, a reduction in the web thickness does not significantly change the α values (an increase from 0.17 to 0.23). On the other hand, a change in the web slenderness, results in a reduction in the buckling capacity. First of all, in order to understand the effects of distortion, the basic case of equal and opposite end moments was analyzed. The results of the analyses are given in Table 3.2. In this table, M_{cr0} values were found by Eqn. 1.1 and these values do not account for cross section distortion. On the other hand, M_{cr}

values obtained from finite element analysis reflects the contribution of the cross section distortion.

Table 3.2 – Comparison of theoretical and finite element analysis results

h/t_w	$M_{cr0} (w-inc)$	$M_{cr0} (FE)$	% Diff.
25	136.3	138.1	-1.4%
40	123.9	119.6	3.5%
60	121.1	107.3	11.4%
80	120.5	95.9	20.4%

Analysis result showed that the buckling capacity can be reduced by 20 percent by increasing the web slenderness value to 80. In order to be able to make comparisons, the critical buckling moments found from finite element analysis are normalized by $M_{cr0} (w-inc)$ without considering the reduction due to web slenderness. The analysis for the cases of $h/t_w=40$, $h/t_w=60$ and $h/t_w=80$ are given in Figs. 3.16 to 3.18.

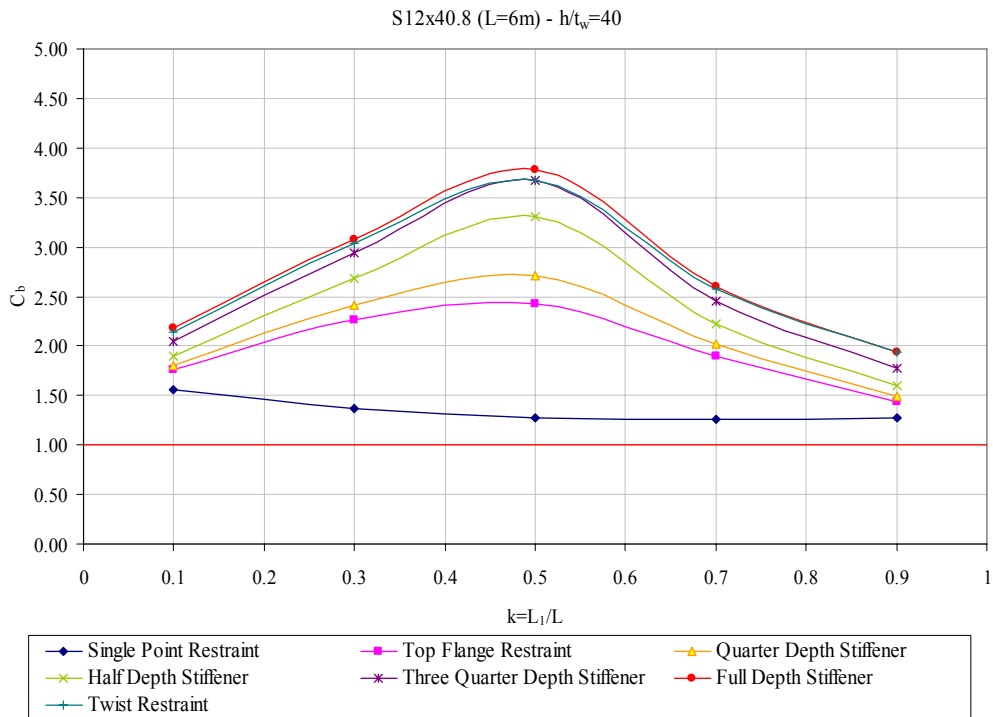


Fig. 3.16 – Comparison of different boundary conditions for S12x40.8 beam with $h/t_w=40$.

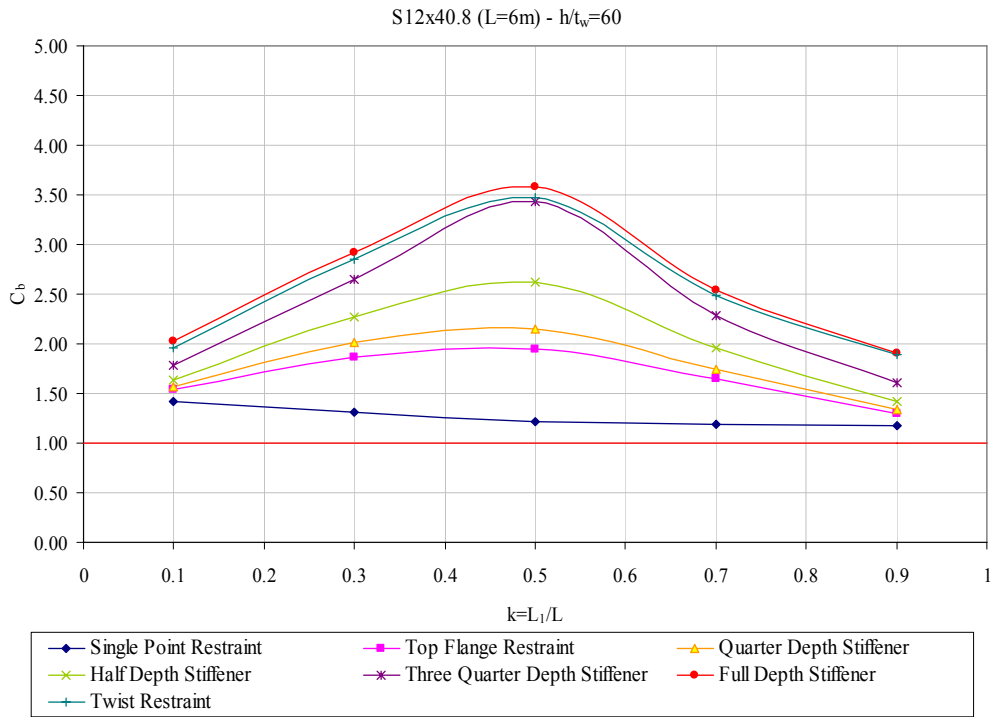


Fig. 3.17 – Comparison of different boundary conditions for S12x40.8 beam with $h/t_w=60$.

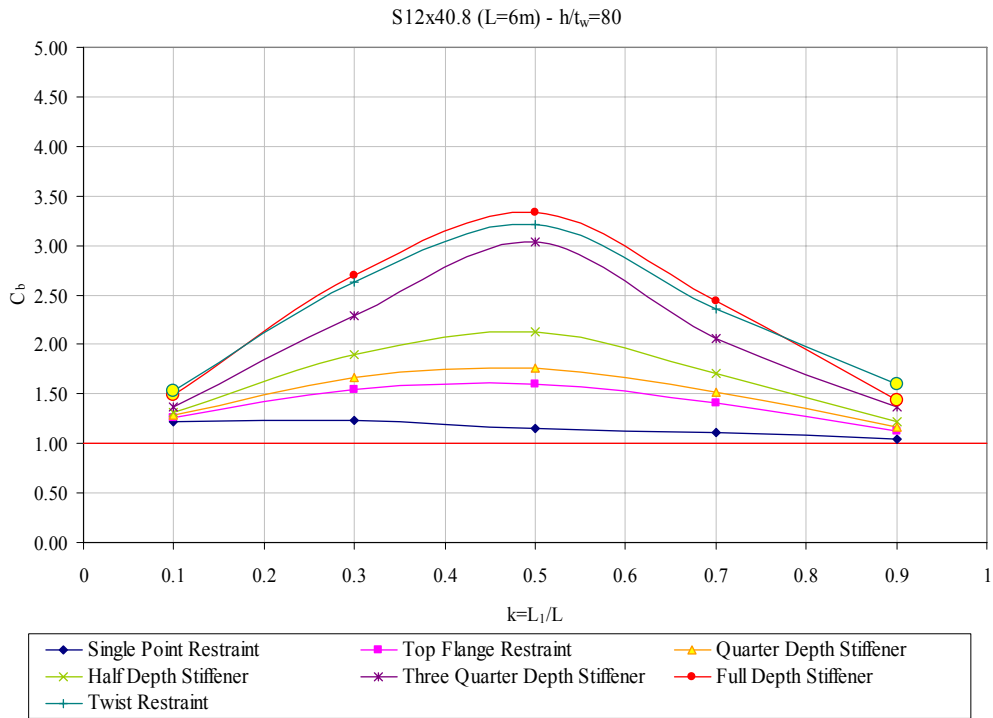


Fig. 3.18 – Comparison of different boundary conditions for S12x40.8 beam with $h/t_w=80$.

In addition, the comparison of sections with different h/t_w values is given in Figs. 3.19 to 3.25 for the seven boundary conditions.

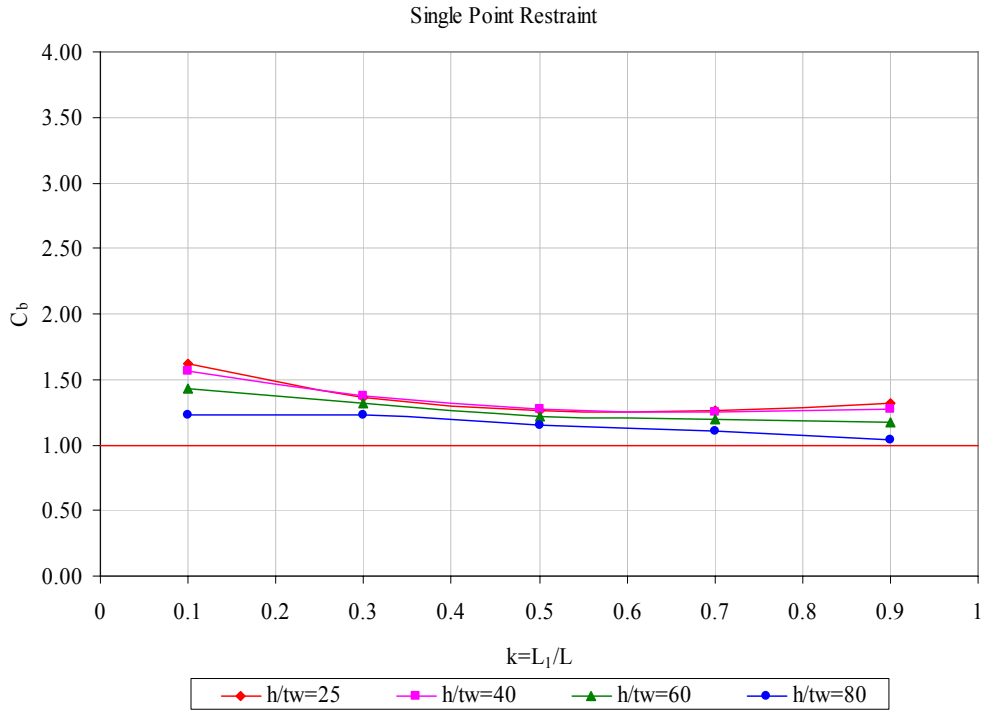


Fig. 3.19 – Comparison of different h/t_w values for single point restraint (SPR) case.

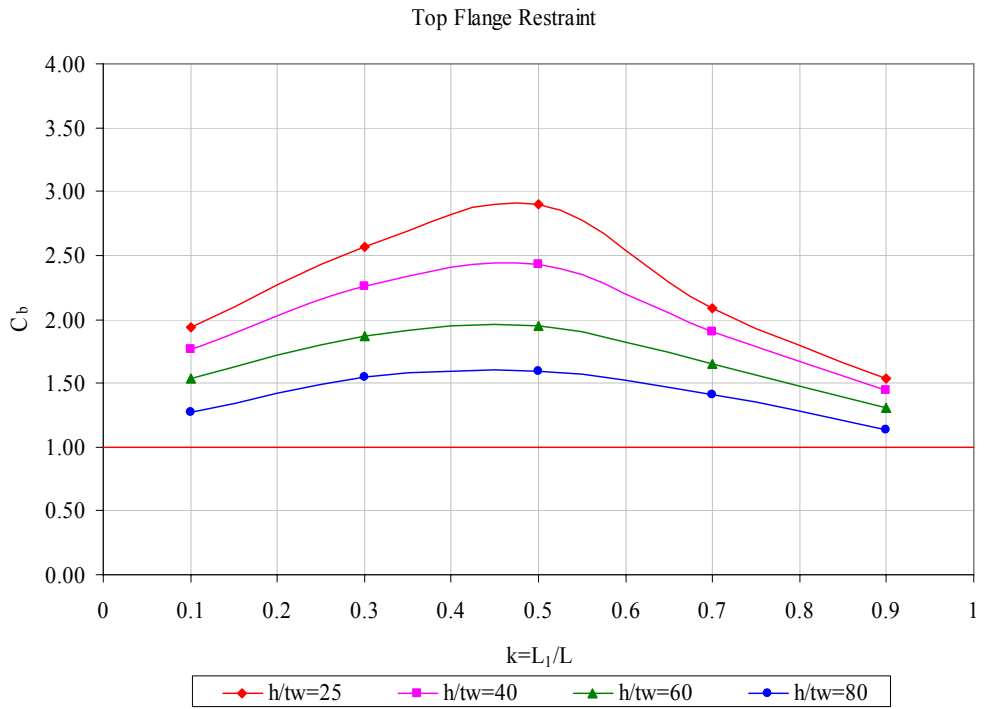


Fig. 3.20 – Comparison of different h/t_w values for top flange restraint (TFR) case.

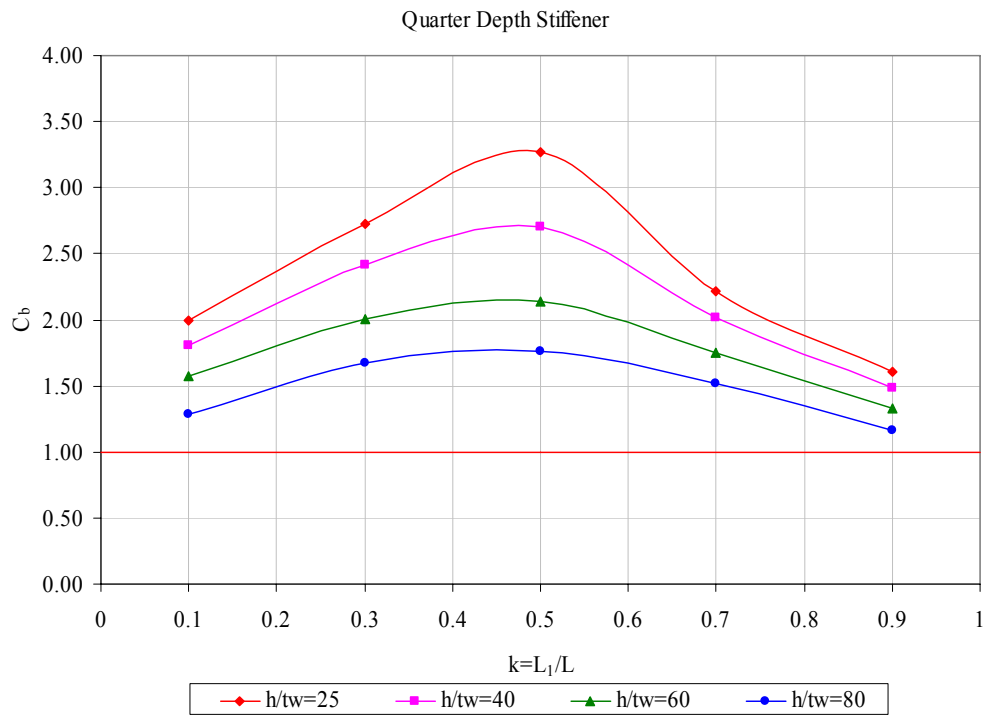


Fig. 3.21 – Comparison of different h/t_w values for quarter depth stiffener (QDS) case.

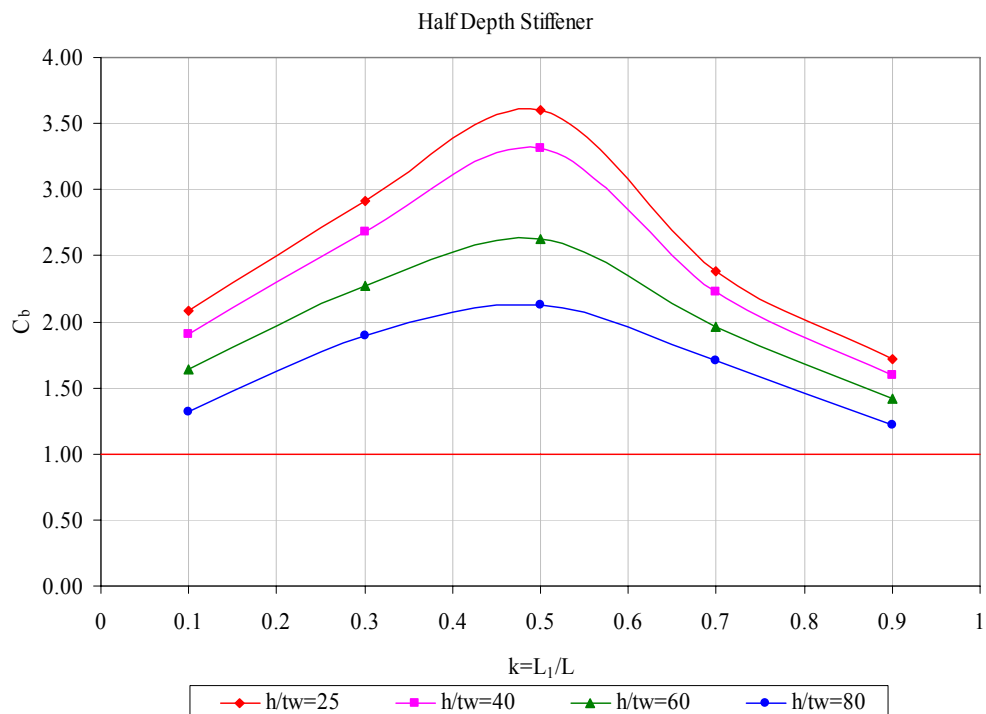


Fig. 3.22 – Comparison of different h/t_w values for half depth stiffener (HDS) case.

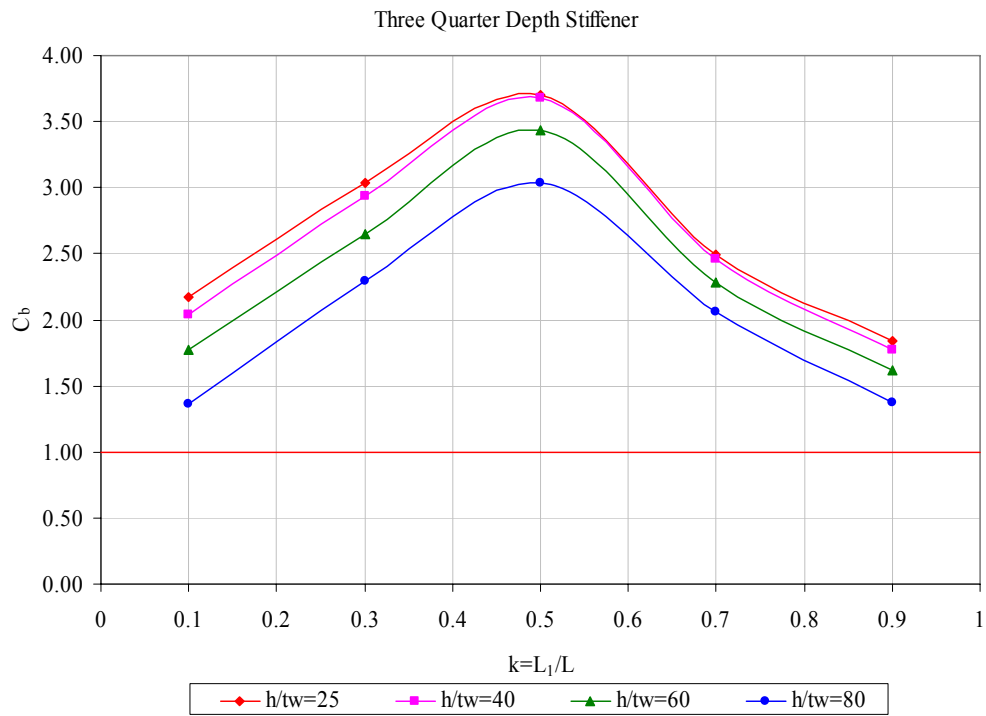


Fig. 3.23 – Comparison of different h/t_w values for three quarter depth stiffener (TQDS) case.

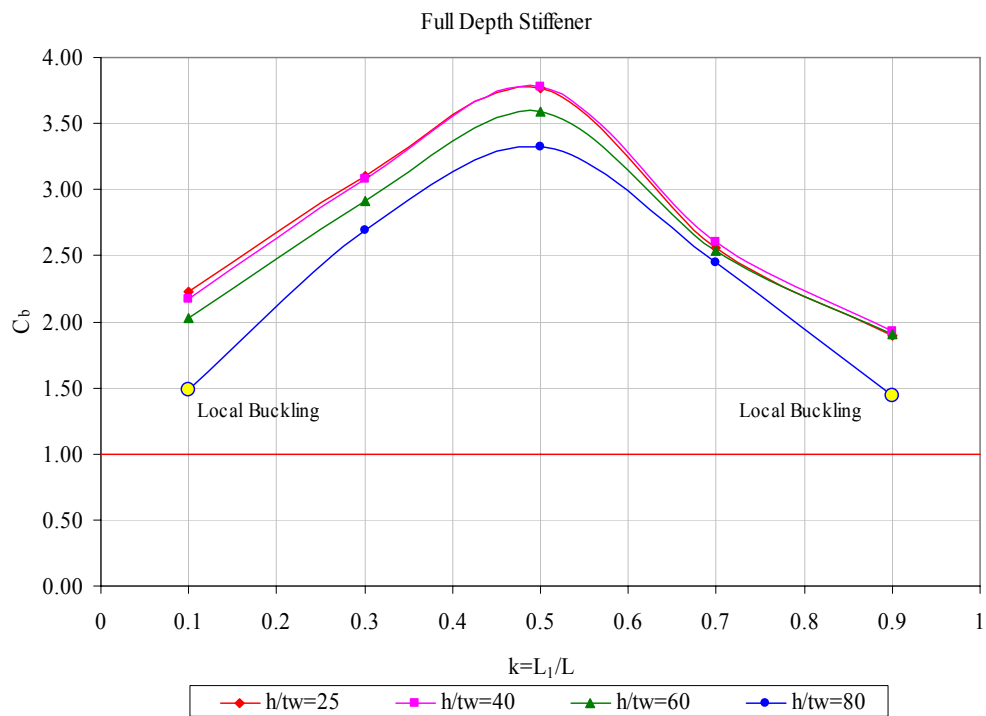


Fig. 3.24 – Comparison of different h/t_w values for full depth stiffener (FDS) case.

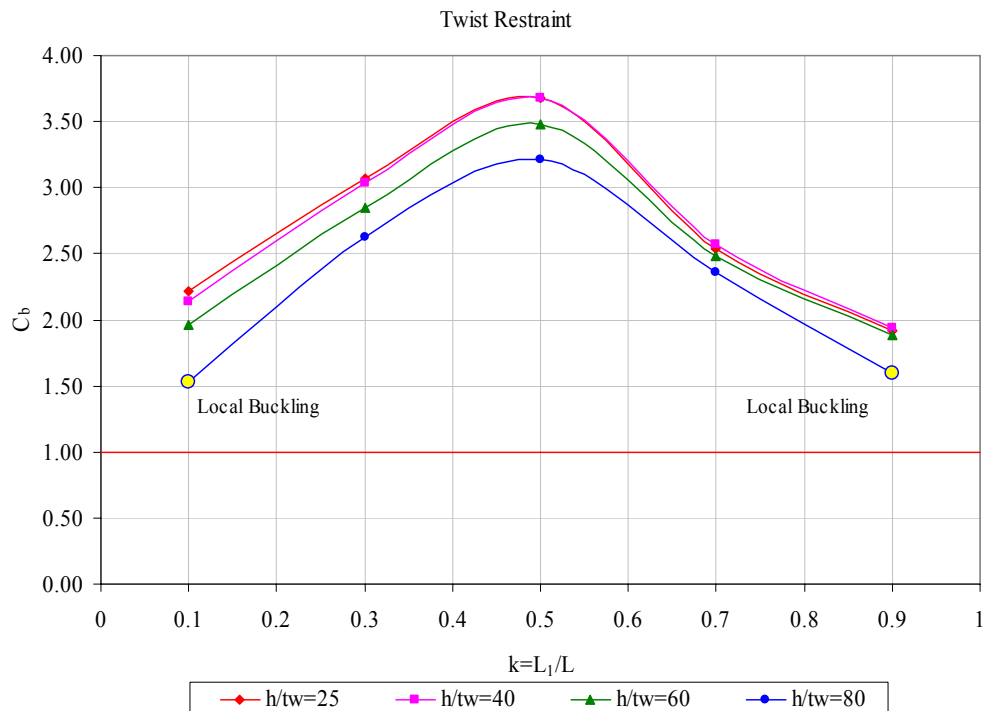


Fig. 3.25 – Comparison of different h/t_w values for twist restraint (TR) case.

Examination of Figs. 3.19 through 3.25 reveals that the buckling capacity reduces as the web gets slender. The percent reduction in capacity is a function of the k value and the boundary conditions. For the single point restraint case, the reduction in capacity is not much pronounced. This is due to the fact that the cross section is allowed to rotate at the exterior support location. For this boundary condition, use of a C_b value equal to unity can be recommended for all k ranges and high h/t_w values.

In order to examine the amount of reduction in capacity for the other boundary conditions, Figs. 3.26 through 3.31 were prepared and local buckling values are excluded. In these figures the percent reduction in capacity is displayed for h/t_w values of 40, 60 and 80. The percent reduction values are computed by considering the $h/t_w=25$ as the base case.

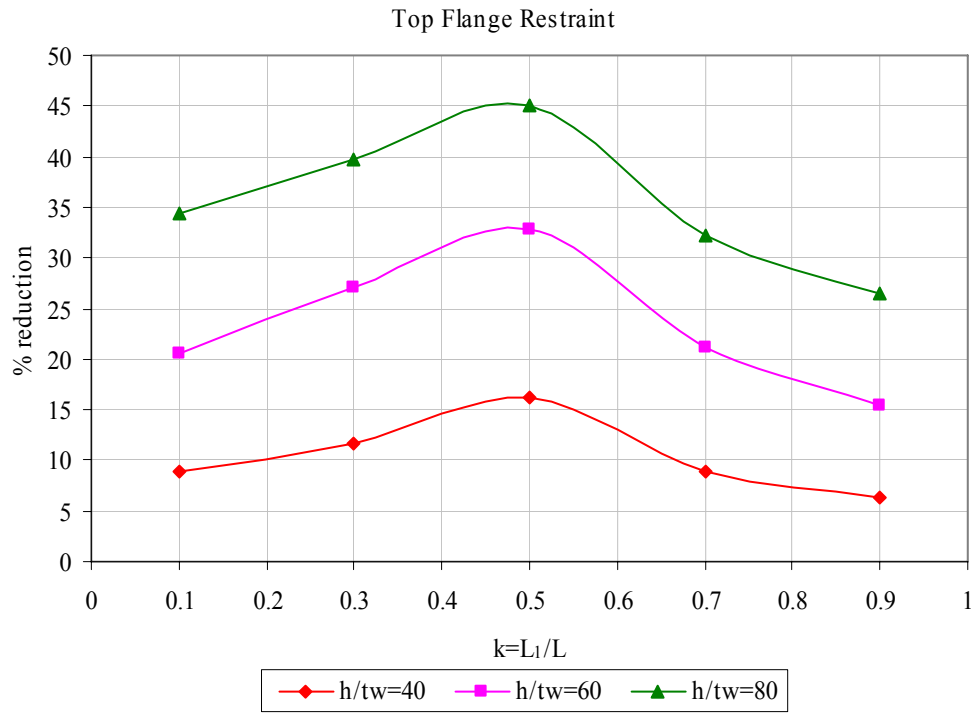


Fig. 3.26 – Percent reduction in capacity for TFR case.

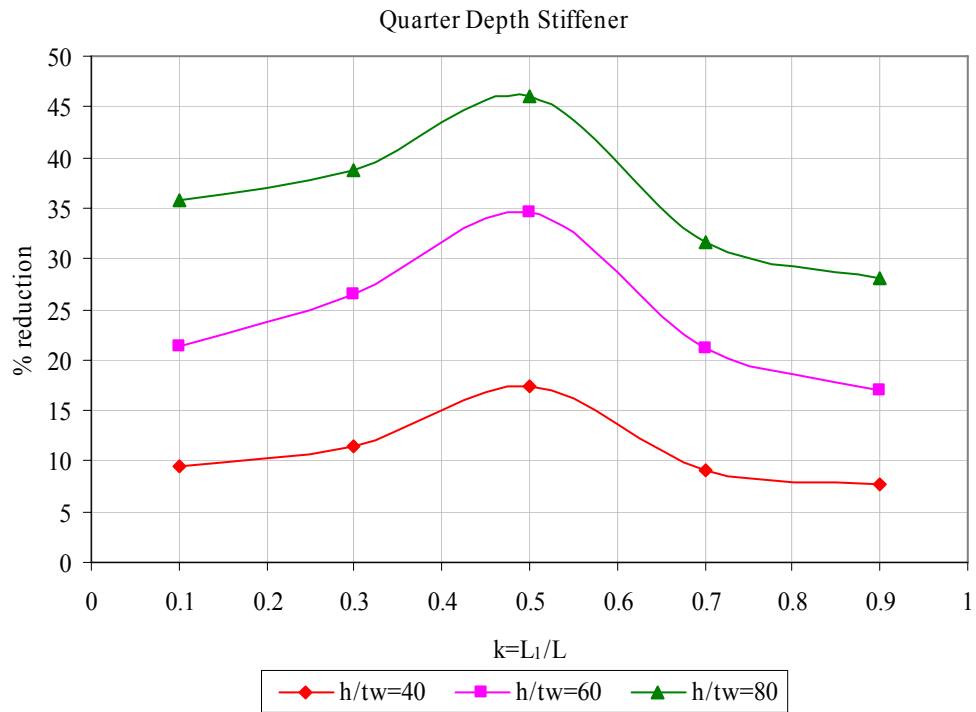


Fig. 3.27 – Percent reduction in capacity for QDS case.

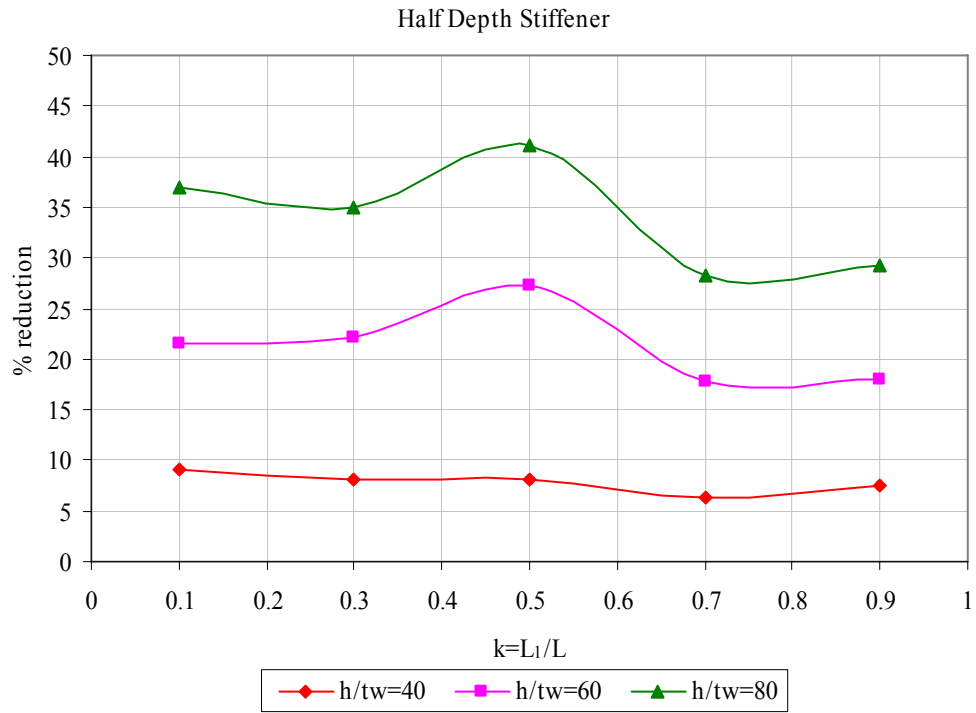


Fig. 3.28 – Percent reduction in capacity for HDS case.

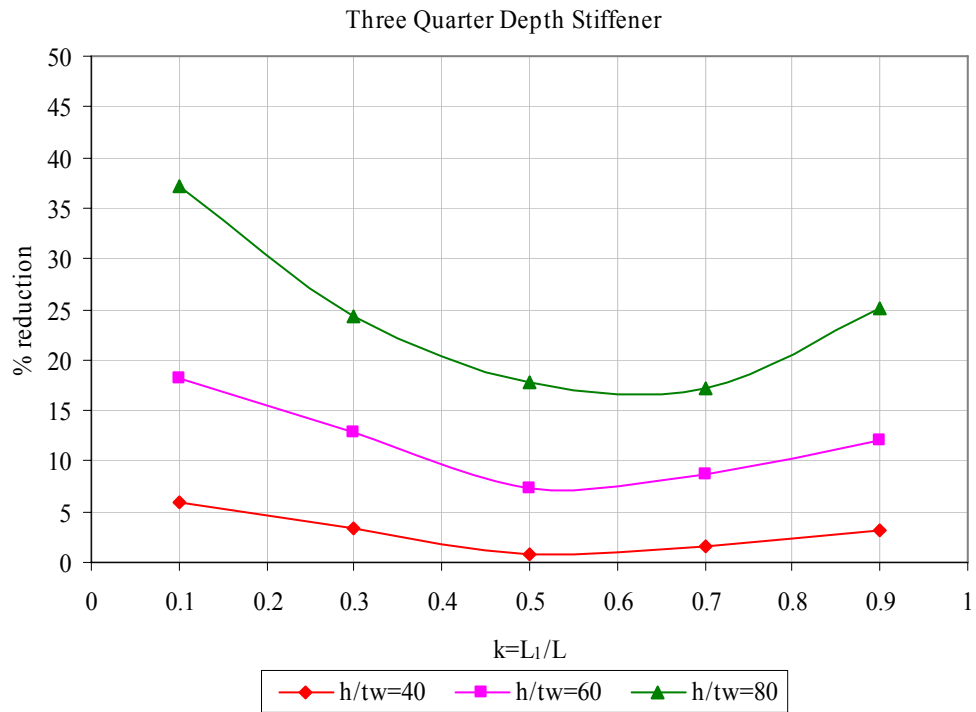


Fig. 3.29 – Percent reduction in capacity for TQDS case.

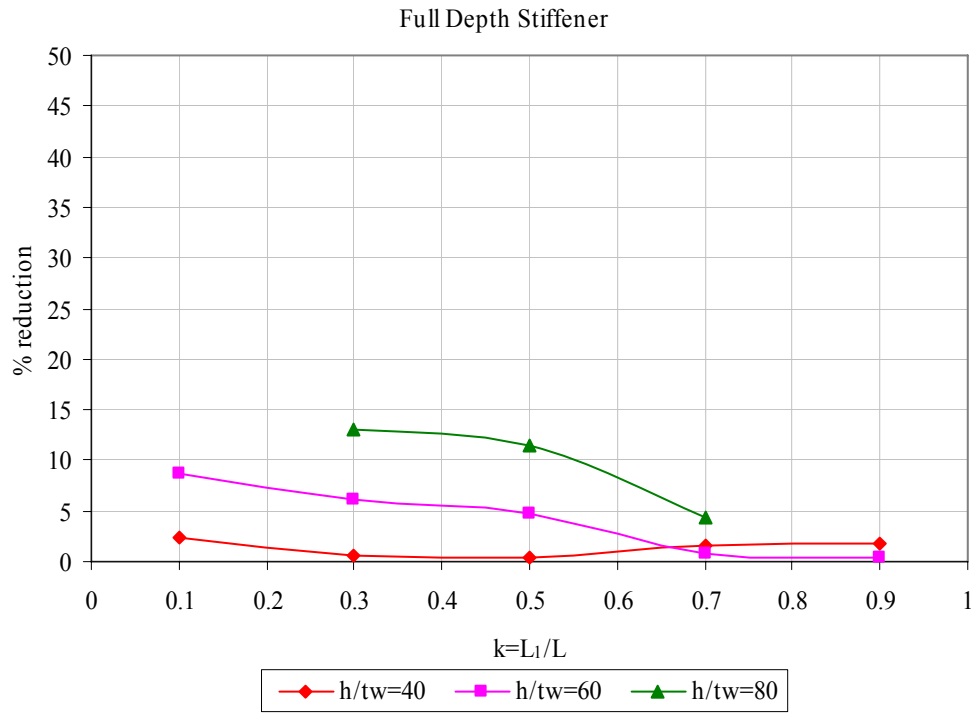


Fig. 3.30 – Percent reduction in capacity for FDS case.

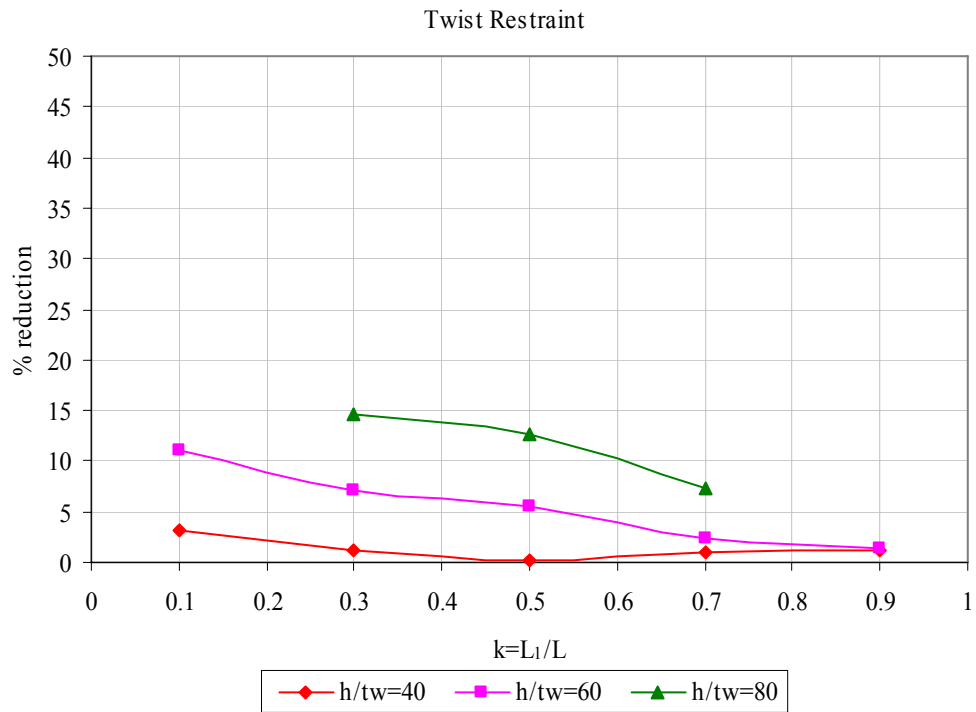


Fig. 3.31 – Percent reduction in capacity for TR case.

When these figures are examined it can be seen that the behavior is similar for the top flange restraint (TFR), quarter depth stiffener (QDS) and half depth stiffener (HDS) cases. The three quarter depth stiffener (TQDS) case exhibits a different behavior compared to the other mentioned three cases. Full depth stiffener (FDS) and twist restraint (TR) cases are not investigated in detail in this section because of the impractical nature of these boundary conditions. It should also be noted that the change in C_b values stay below 15 percent for these cases.

According to these observations, a reduction factor for C_b needs to be developed for sections having high h/t_w values. There has to be different reduction factors depending on the boundary conditions. Based on the observations, the TFR, QDS and HDS can be grouped together. By curve fitting to the data for these three boundary conditions, various equations with different complexity could be developed. In this thesis, two equations (Eqn. 3.4 and Eqn. 3.5) were derived for the reduction factor for h/t_w values greater than 25.

For TFR, QDS and HDS and $h/t_w > 25$,

$$RF = 0.15 + 0.6 \left(\frac{h/t_w - 55}{100} \right) \quad (3.4)$$

$$RF = \frac{(-40k^2 + 37k + 14)}{100} \left(\frac{h/t_w}{25} - 1 \right) \quad (3.5)$$

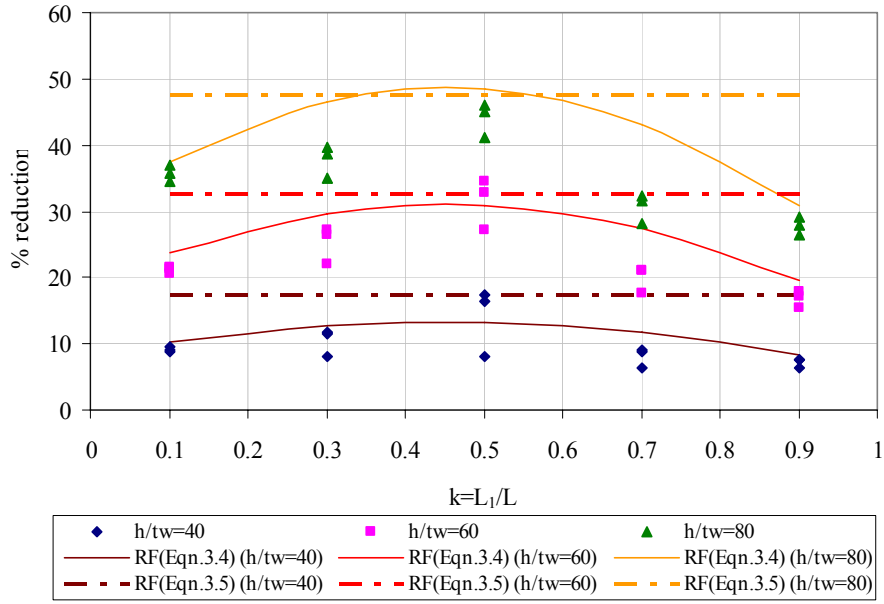


Fig. 3.32 – Percent reduction values for TFR, QDS and HDS cases.

The quality of the developed equation is presented in Fig. 3.32. In this figure, the data points that belong to the TFR, QDS and HDS cases are compared against predictions of the developed equation. For the TQDS case, similar type of curve fitting was performed and the following equation was developed.

For TQDS and $h/t_w > 25$,

$$RF = \frac{(37k^2 - 43k + 21)}{100} \left(\frac{h}{t_w} - 1 \right) \quad (3.6)$$

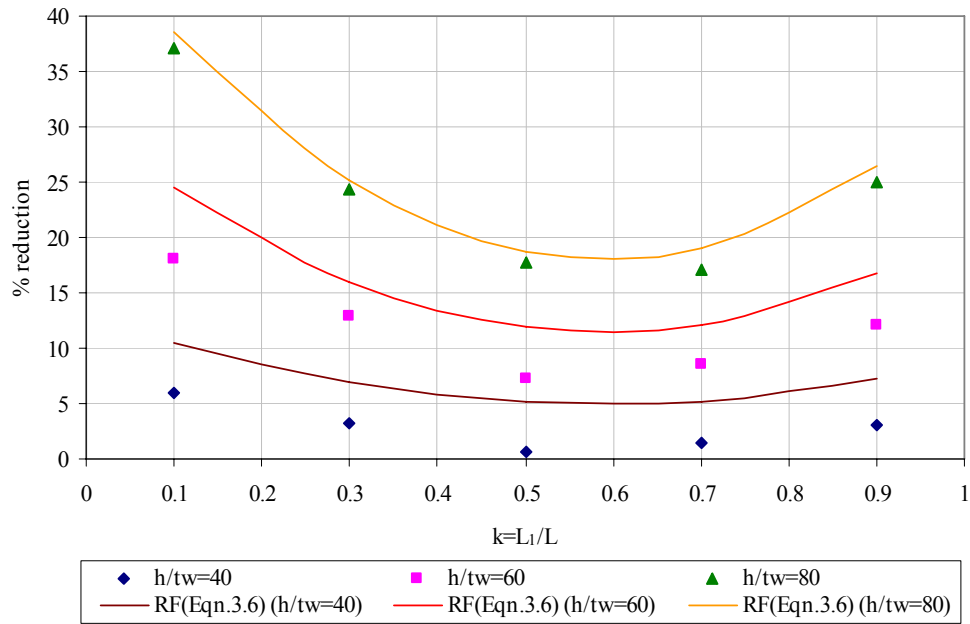


Fig. 3.33 – Percent reduction values for TQDS case.

The quality of the developed equation is presented in Fig. 3.33. The developed Eqns. 3.4, 3.5 and 3.6 can be used together with the Eqn. 3.3 to estimate the C_b value for beams with h/t_w values greater than 25.

3.4 A CAVEAT ON LOCAL BUCKLING

Analyses presented so far were limited to certain beam geometries due to the possibility of local buckling. Even few of the data points presented were influenced by local buckling. When the elements of the cross section (web or flange) are subjected to compression or shear, local buckling can occur for high slenderness values. Buckling of plates under axial and shear stresses has been studied extensively in the past (Timoshenko and Gere, 1961). The critical stress is found by the following equation.

$$\sigma_{cr} = \frac{K\pi^2 E}{12(1-\nu^2)(b/t)^2} \quad (3.6)$$

where: K : plate buckling coefficient
 ν : Poisson's ratio
 b : width of the compression element
 t : thickness of the compression element

Depending on the slenderness of the web and flange plates, local web buckling due to shear and/or bending or local flange buckling may occur. Unfortunately, it is difficult to forecast whether local buckling will precede the global lateral buckling. The lateral buckling capacity has been known to come up with a decision. Therefore, a trial and error procedure is used in selecting the sections appropriate for lateral buckling analysis.

Several other sections were tried during the course of the study (S12x40.8 with $h/t_w=100, 120, 140, 160, 180$; SEC1 with $L=3\text{m}$; SEC2 with $L=3\text{m}$). Unfortunately, their behavior was influenced by local effects. Due to this reason, analysis results pertaining to these sections are not presented in the thesis. Representative local buckling shapes are given in Fig 3.34.

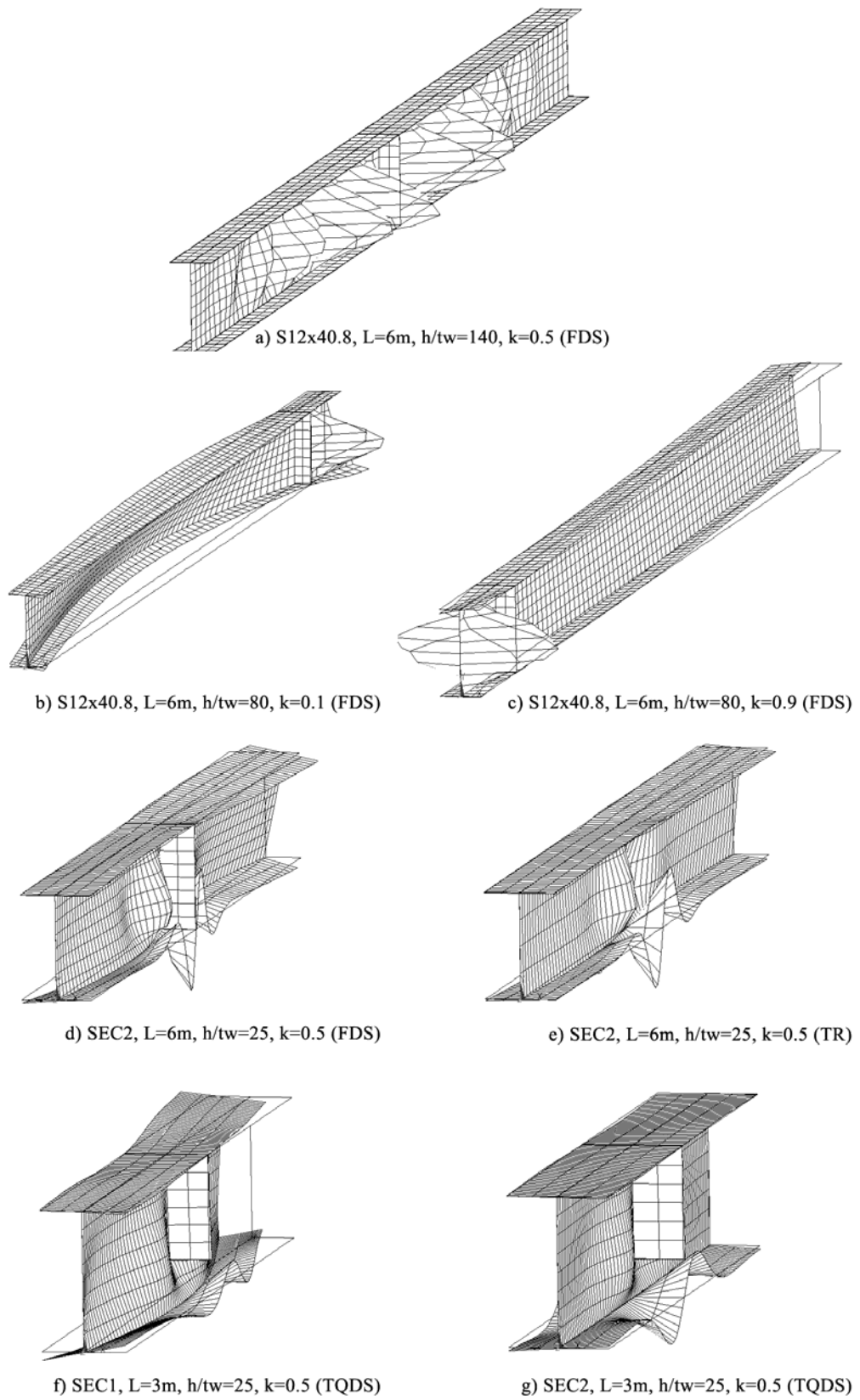


Fig. 3.34 – Local buckling effects occurred during analyses.

CHAPTER 4

ANALYSIS OF A DOUBLE OVERHANGING MONORAIL

4.1 COMPARISON OF SINGLE AND DOUBLE OVERHANGING BEAMS

In the previous chapter, it is seen that the boundary conditions at the exterior support have a significant effect on the capacity of the beam, and except the single point restraint case, all other 6 cases acts in the same behavior in the C_b comparison figures. Also the effect of warping term is investigated by analyzing sections with greater warping contributions. Conservative lower bound equations were developed for practical purposes instead of complicated design equations. Furthermore, the effects of web distortion were investigated and the percent reduction in capacity for the boundary conditions was obtained to give a reduction factor for higher h/t_w values than 25. In this chapter, a comparison analysis is carried out for single overhanging beams and double overhanging beams.

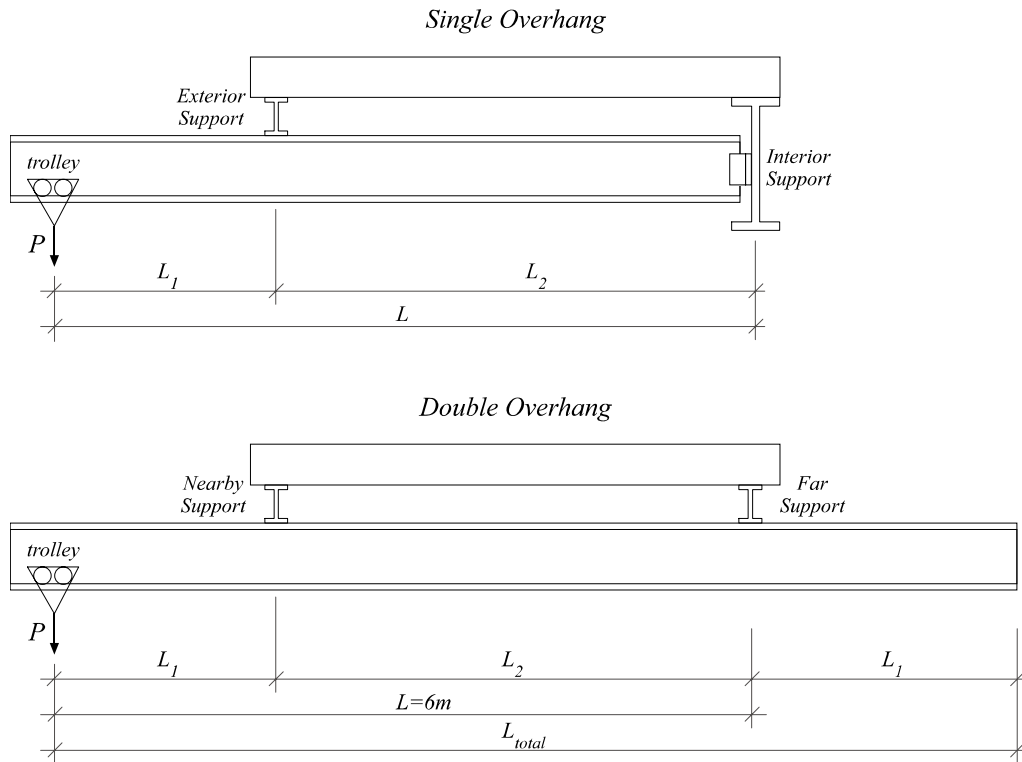


Fig. 4.1 – Typical single and double overhanging monorails.

For double overhanging beam, the system is supposed to be symmetric in structure but loading is acted on only one side of the beam for the worst case as shown in Fig. 4.1. Same S12x40.8 section is used and for comparison with single overhanging model, the length between the load and the last support is taken as 6m. The second overhanging part is taken as L_1 for symmetry purposes so the length of the second overhang is changed with the change in the k value.

Comparison of single and double overhanging beam for different boundary conditions is given in Figs. 4.2 through 4.7. In the single point restraint (SPR) case, both supports are unrestrained against rotation so the system becomes unstable. For this reason, the single point restraint (SPR) case is excluded in analyses due to the instability caused by the support condition.

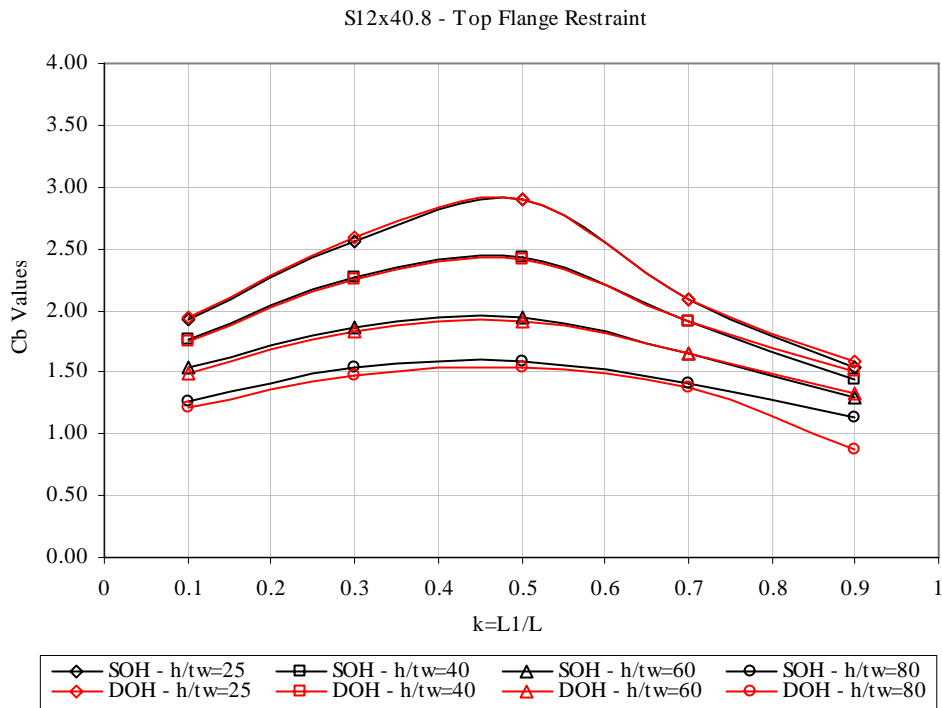


Fig. 4.2 – Comparison of single and double overhanging beams for TFR case.

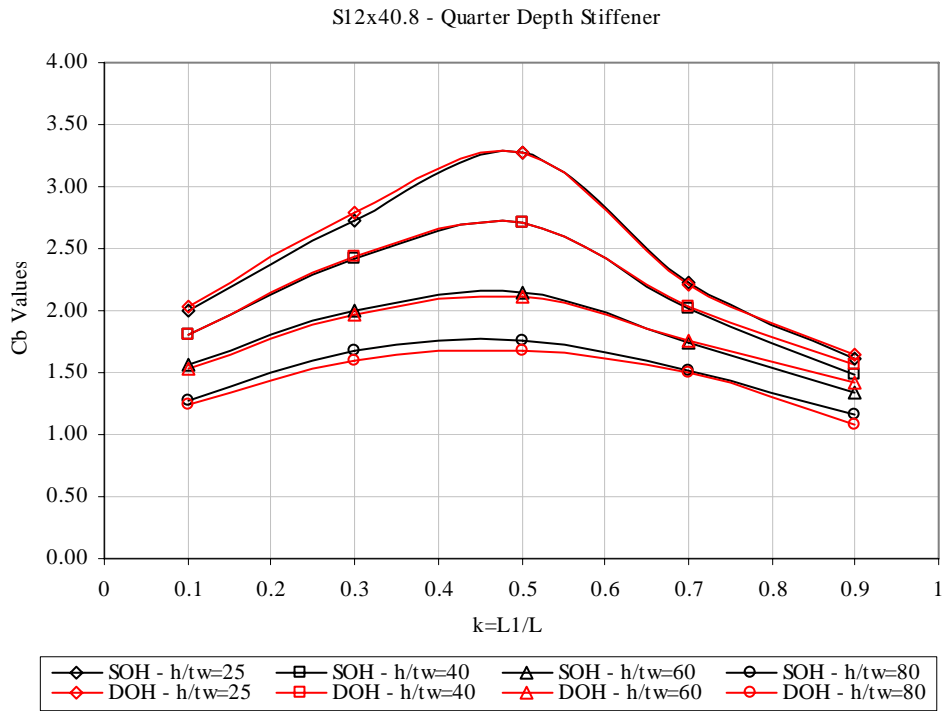


Fig. 4.3 – Comparison of single and double overhanging beams for QDS case.

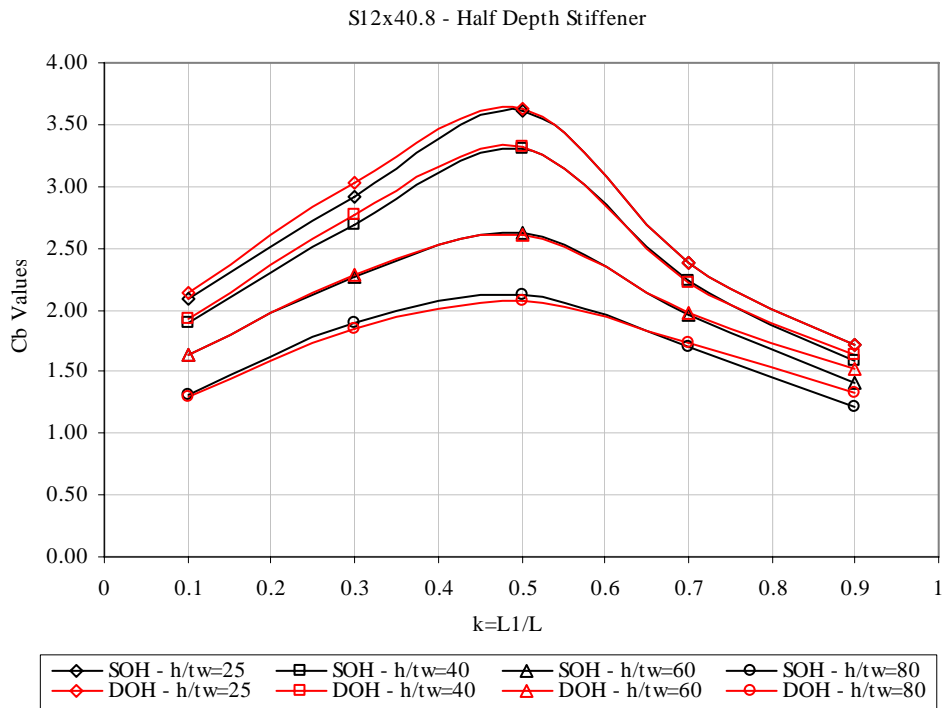


Fig. 4.4 – Comparison of single and double overhanging beams for HDS case.

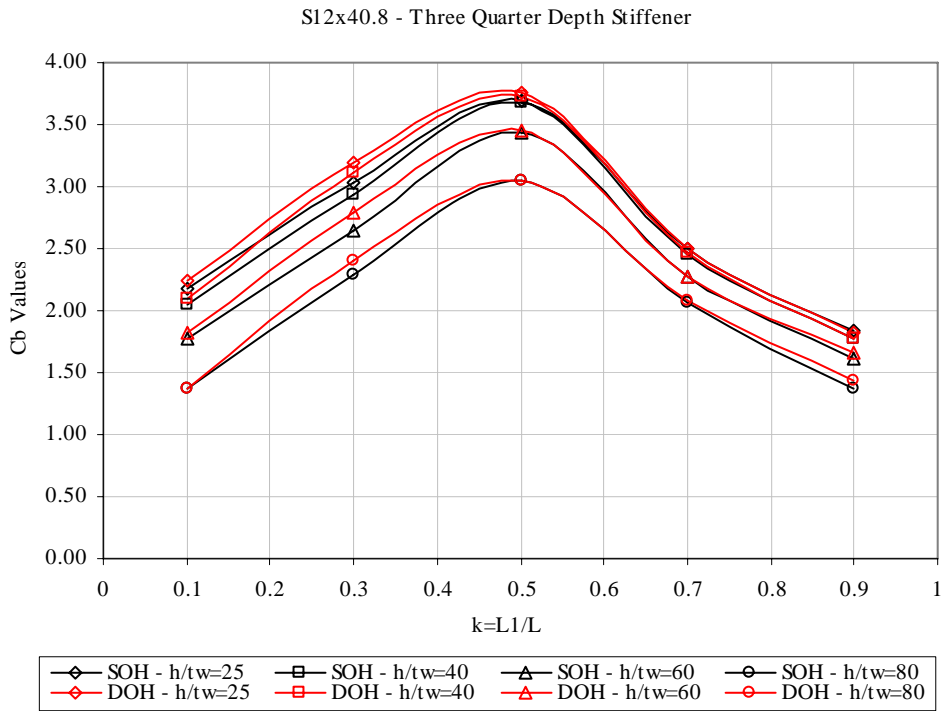


Fig. 4.5 – Comparison of single and double overhanging beams for TQDS case.

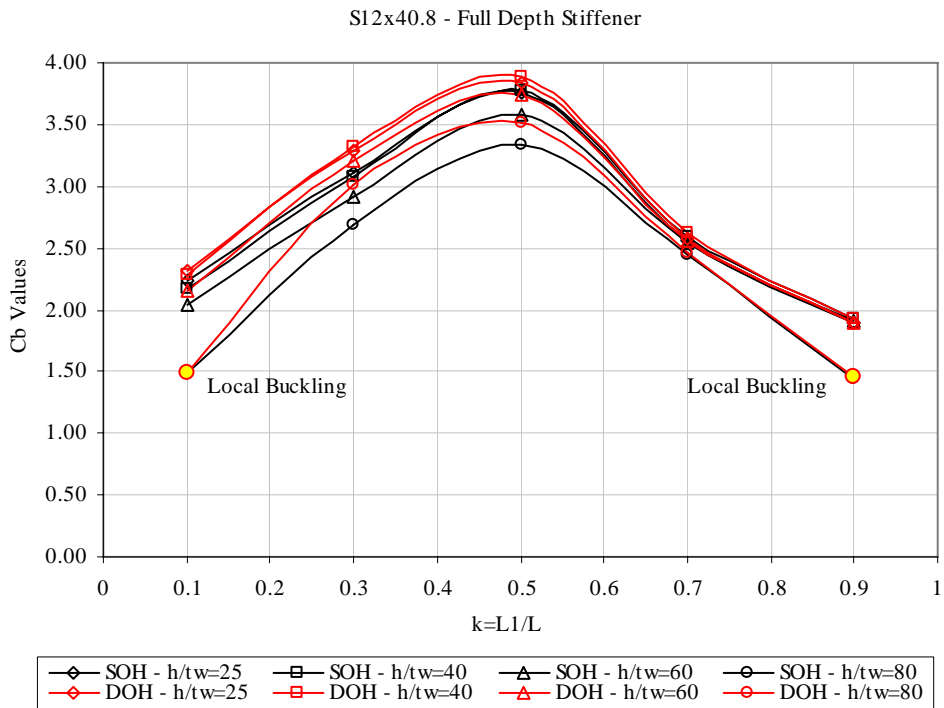


Fig. 4.6 – Comparison of single and double overhanging beams for FDS case.

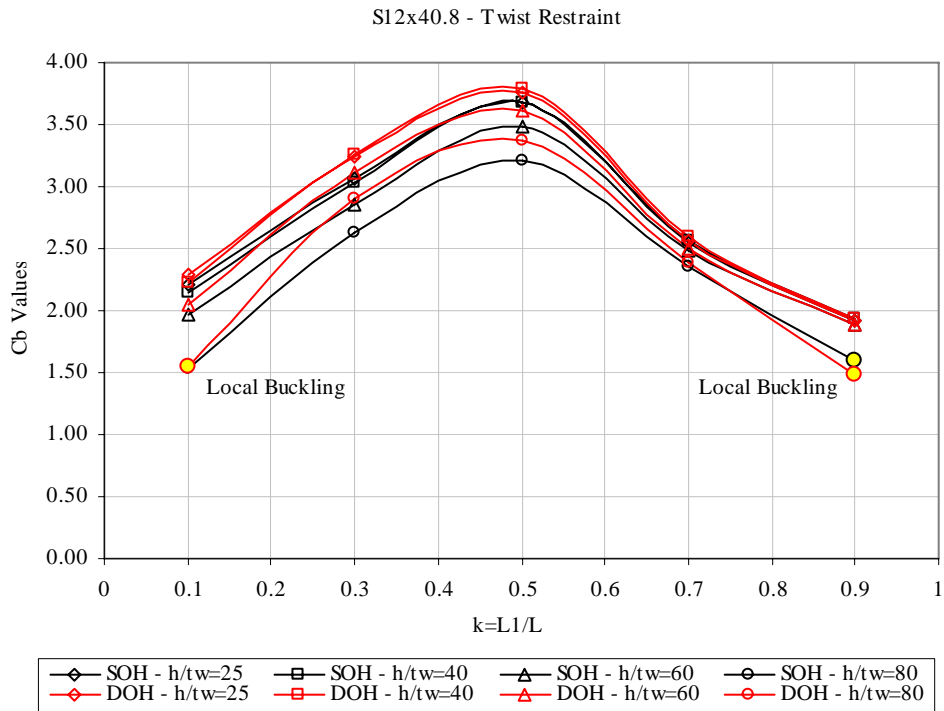


Fig. 4.7 – Comparison of single and double overhanging beams for TR case.

When the comparison graphs are examined, it is seen that there exists an acceptably small difference between single and double overhanging beams. Therefore, the conclusions and expressions attained in previous chapter for single overhanging beams are also valid for double overhanging beams.

CHAPTER 5

SUMMARY AND CONCLUSIONS

5.1 SUMMARY

Lateral torsional buckling of overhanging crane trolley monorails has not been studied in detail. Previous research has focused on the solution of buckling capacities of overhanging monorails under idealized boundary and loading conditions. In this thesis, the buckling of overhanging monorails was studied in detail. First, the effects of load position and support location among the cross section were investigated and the results were compared with the findings of previous research. Then, a detailed analysis of boundary conditions at exterior support was conducted. In addition, the performance of beams having different warping and torsional stiffness properties were investigated. The influence of cross section distortion on buckling capacity of overhanging monorails was explored. Finally, the investigations performed for single overhanging beams were extended to double overhanging beams.

5.2 CONCLUSIONS

The following could be concluded from this study:

- Buckling of overhanging monorails are greatly influenced by the location of loading and supports on the cross-section. Realistic conditions considering bottom flange loading and exterior support at top flange yield in much higher buckling capacities as compared to idealized load and boundary conditions (support and loading at shear centre).
- When boundary conditions preventing the vertical moment of the top flange at exterior support location are considered even higher buckling capacities could be attained. Buckling capacity tends to increase with an increase in the depth of the stiffener placed at exterior support.

- Sections having different torsional and warping properties exhibit different responses, however, the C_b values obtained for different sections are close to each other. Based on this observation, simple expressions were developed for predicting C_b values for different boundary conditions.
- Buckling capacity of overhanging monorails tend to decrease as the web slenderness increases. Simple design recommendations were developed for predicting the reduction in buckling capacity due to increasing web slenderness.
- Conclusions drawn for single overhanging monorails are valid for double overhanging monorails. The effect of different boundary conditions at interior support has negligible effect on the buckling capacity.
- Future research should extend the findings of this study to different cross section geometries. Monosymmetric sections and tapered overhanging beams require additional treatment. This study focused on the case where the loading is at the tip of the overhanging segment. Additional studies are required to investigate the instability of these systems under a point load at the mainspan.

REFERENCES

AISC, *Load and Resistance Factor Design Specification for Structural Steel Buildings*, American Institute of Steel Construction, Third Edition, Chicago, Illinois, 2001.

ANSYS Version 7.0 On-line User's Manual, 2003.

Bradford, M. A., and Trahair, N. S., *Distortional buckling of I-beams*, Journal of the Structural Division, ASCE, Vol. 107, No. ST2, 1981, pp355-370

Bradford, M. A., *Lateral distortional buckling of steel I-section members*, Journal of Constructional Steel Research, Vol. 23, 1992, pp97-116

Bradford, M. A., *Elastic distortional buckling of overhanging beams*, UNICIV Report, No.R-337, The University of New South Wales, Sydney, Australia, 1994.

Essa, H. S., and Kennedy, D. J. L., *Design of Cantilever Steel Beams Refined Approach*, J. Struct. Eng., ASCE, Vol. 120, No. 9, 1994, pp2623-2636

Nethercot, D. A., *The effective lengths of cantilevers as governed by lateral buckling*, The Structural Engineer, Vol. 51, No. 5, 1973, pp161-168

Pi, Y.-L., and Trahair, N. S., *Distortion and warping at beam supports*, Journal of Structural Engineering, ASCE, Vol. 126, No. 11, 2000, pp1279-1287

Tanner, N. S., *Allowable bending stresses for overhanging monorails*, Engineering Journal, AISC, Third Quarter, 1985, pp133-138

Timoshenko S. P., and Gere J. M., *Theory of elastic stability*, 2nd Edition, McGraw-Hill, New York, N. Y., 1961.

Trahair, N. S., *Lateral buckling of overhanging beams*, Proc., Int. Conf. Instability and Plastic Collapse of Steel Structures, L. J. Morris, ed., Granada Publishing, London, England, 1983.

TS 648, *Building code for steel structures*, Ankara, Turkey, 1980.

APPENDIX A

TABULAR DATA FOR GRAPHS

2.2 VERIFICATION OF FINITE ELEMENT RESULTS

Table A2.4 – The comparison chart of Tanner’s findings (1985) and analysis results.

		Middle Support Middle Loading Case		
L_1 (mm)	$k=L_1/L$	C_b Values (w-inc)	C_b Values (w-exc)	C_b Values From Tanner's Paper
6000	1.0			1.28
5400	0.9	1.05	1.14	1.15
4800	0.8	0.96	1.04	1.05
4200	0.7	0.88	0.95	0.96
3600	0.6	0.81	0.88	0.90
3000	0.5	0.76	0.82	0.84
2400	0.4	0.72	0.77	0.80
1800	0.3	0.67	0.73	0.76
1200	0.2	0.63	0.68	0.73
600	0.1	0.53	0.58	0.70
0	0.0			0.67

2.3 EFFECTS OF LOADING AND BOUNDARY CONDITIONS

Table A2.5 – Comparison chart of Tanner’s findings (1985) and analysis results for different loading and boundary conditions

	MSML	MSBL	TSML	TSBL	
$k=L_1/L$	C_b (w-inc)	C_b (w-inc)	C_b (w-inc)	C_b (w-inc)	C_b Values From Tanner's Paper
1.0					1.28
0.9	1.05	1.20	1.15	1.31	1.15
0.8	0.96	1.09	1.11	1.29	1.05
0.7	0.88	1.01	1.08	1.26	0.96
0.6	0.81	0.96	1.05	1.25	0.90
0.5	0.76	0.93	1.04	1.26	0.84
0.4	0.72	0.91	1.04	1.29	0.80
0.3	0.67	0.93	1.08	1.36	0.76
0.2	0.63	0.99	1.17	1.48	0.73
0.1	0.53	1.17	1.37	1.62	0.70
0.0					0.67

3.1 INSTABILITY UNDER DIFFERENT BOUNDARY CONDITIONS AT EXTERIOR SUPPORT

Table A3.2 – Comparison of different boundary conditions for S12x40.8 beam with 6m length.

$k=L_1/L$	C_b Value [Normalized with $M_{cr0} (w-inc)$]						
	SPR	TFR	QDS	HDS	TQDS	FDS	TR
0.1	1.62	1.93	2.00	2.09	2.17	2.23	2.21
0.3	1.36	2.56	2.73	2.92	3.03	3.10	3.07
0.5	1.26	2.90	3.27	3.61	3.70	3.76	3.68
0.7	1.26	2.09	2.22	2.38	2.49	2.56	2.54
0.9	1.31	1.54	1.61	1.72	1.83	1.90	1.91

3.2 INFLUENCE OF WARPING AND TORSIONAL STIFFNESS

Table A3.5 – Comparison of different boundary conditions for S12x40.8 beam with 3m length.

$k=L_1/L$	C_b Value [Normalized with $M_{cr0} (w-inc)$]						
	SPR	TFR	QDS	HDS	TQDS	FDS	TR
0.1	1.69	1.77	1.82	1.92	2.10	2.27	2.28
0.3	1.66	2.23	2.48	2.87	3.27	3.51	3.53
0.5	1.55	2.36	2.76	3.59	4.42	4.52	4.43
0.7	1.45	1.93	2.14	2.49	2.86	3.09	3.14
0.9	1.37	1.48	1.54	1.67	1.93	2.18	2.31

Table A3.6 – Comparison of different boundary conditions for SEC1 beam with 6m length.

$k=L_1/L$	C_b Value [Normalized with $M_{cr0} (w-inc)$]						
	SPR	TFR	QDS	HDS	TQDS	FDS	TR
0.1	1.73	1.80	1.84	1.94	2.13	2.34	2.32
0.3	1.75	2.31	2.54	2.94	3.40	3.69	3.70
0.5	1.64	2.46	2.85	3.68	4.66	4.77	4.68
0.7	1.51	2.00	2.21	2.58	3.02	3.31	3.33
0.9	1.40	1.50	1.56	1.70	2.00	2.34	2.44

Table A3.7 – Comparison of different boundary conditions for SEC2 beam with 6m length.

$k=L_1/L$	C_b Value [Normalized with $M_{cr0} (w-inc)$]						
	SPR	TFR	QDS	HDS	TQDS	FDS	TR
0.1	1.71	1.74	1.77	1.85	2.02	2.28	2.29
0.3	1.81	2.13	2.34	2.70	3.19	3.71	3.74
0.5	1.73	2.26	2.60	3.24	3.86	4.42	3.99
0.7	1.56	1.88	2.08	2.44	2.96	3.45	3.49
0.9	1.39	1.45	1.49	1.61	1.90	2.39	2.55

Table A3.8 – Comparison of different sections for single point restraint (SPR) case.

$k=L_1/L$	S12x40.8 ($\alpha=0.17$ & L=6m)	S12x40.8 ($\alpha=0.70$ & L=3m)	SEC1 ($\alpha=1.04$ & L=6m)	SEC2 ($\alpha=2.09$ & L=6m)	Predictory Eqn.
0.1	1.62	1.83	1.73	1.71	1.45
0.3	1.36	1.75	1.75	1.81	1.35
0.5	1.26	1.62	1.64	1.73	1.25
0.7	1.26	1.54	1.51	1.56	1.15
0.9	1.31	1.48	1.40	1.39	1.05

Table A3.9 – Comparison of different sections for top flange restraint (TFR) case.

$k=L_1/L$	S12x40.8 ($\alpha=0.17$ & L=6m)	S12x40.8 ($\alpha=0.70$ & L=3m)	SEC1 ($\alpha=1.04$ & L=6m)	SEC2 ($\alpha=2.09$ & L=6m)	Predictory Eqn.
0.1	1.93	1.77	1.80	1.74	1.61
0.3	2.56	2.23	2.31	2.13	2.05
0.5	2.90	2.36	2.46	2.26	2.15
0.7	2.09	1.93	2.00	1.88	1.89
0.9	1.54	1.48	1.50	1.45	1.29

Table A3.10 – Comparison of different sections for quarter depth stiffener (QDS) case.

$k=L_1/L$	S12x40.8 ($\alpha=0.17$ & L=6m)	S12x40.8 ($\alpha=0.70$ & L=3m)	SEC1 ($\alpha=1.04$ & L=6m)	SEC2 ($\alpha=2.09$ & L=6m)	Predictory Eqn.
0.1	2.00	1.82	1.84	1.77	1.70
0.3	2.73	2.48	2.54	2.34	2.26
0.5	3.27	2.76	2.85	2.60	2.38
0.7	2.22	2.14	2.21	2.08	2.06
0.9	1.61	1.54	1.56	1.49	1.30

Table A3.11 – Comparison of different sections for half depth stiffener (HDS) case.

$k=L_1/L$	S12x40.8 ($\alpha=0.17$ & L=6m)	S12x40.8 ($\alpha=0.70$ & L=3m)	SEC1 ($\alpha=1.04$ & L=6m)	SEC2 ($\alpha=2.09$ & L=6m)	Predictory Eqn.
0.1	2.09	1.92	1.94	1.85	1.87
0.3	2.92	2.87	2.94	2.70	2.66
0.5	3.61	3.59	3.68	3.24	2.83
0.7	2.38	2.49	2.58	2.44	2.38
0.9	1.72	1.67	1.70	1.61	1.31

Table A3.12 – Comparison of different sections for three quarter depth stiffener (TQDS) case.

$k=L_1/L$	S12x40.8 ($\alpha=0.17$ & L=6m)	S12x40.8 ($\alpha=0.70$ & L=3m)	SEC1 ($\alpha=1.04$ & L=6m)	SEC2 ($\alpha=2.09$ & L=6m)	Predictory Eqn.
0.1	2.17	2.10	2.13	2.02	2.03
0.3	3.03	3.27	3.40	3.19	3.02
0.5	3.70	4.42	4.66	3.86	3.23
0.7	2.49	2.86	3.02	2.96	2.67
0.9	1.83	1.93	2.00	1.90	1.33

Table A3.13 – Comparison of different sections for full depth stiffener (FDS) case.

$k=L_1/L$	S12x40.8 ($\alpha=0.17$ & L=6m)	S12x40.8 ($\alpha=0.70$ & L=3m)	SEC1 ($\alpha=1.04$ & L=6m)	SEC2 ($\alpha=2.09$ & L=6m)	Predictory Eqn.
0.1	2.23	2.27	2.34	2.28	2.04
0.3	3.10	3.51	3.69	3.71	3.04
0.5	3.76	4.52	4.77	4.42	3.25
0.7	2.56	3.09	3.31	3.45	2.68
0.9	1.90	2.18	2.34	2.39	1.33

Table A3.14 – Comparison of different sections for twist restraint (TR) case.

$k=L_1/L$	S12x40.8 ($\alpha=0.17$ & L=6m)	S12x40.8 ($\alpha=0.70$ & L=3m)	SEC1 ($\alpha=1.04$ & L=6m)	SEC2 ($\alpha=2.09$ & L=6m)	Predictory Eqn.
0.1	2.21	2.28	2.32	2.29	2.05
0.3	3.07	3.53	3.70	3.74	3.06
0.5	3.68	4.43	4.68	3.99	3.28
0.7	2.54	3.14	3.33	3.49	2.70
0.9	1.91	2.31	2.44	2.55	1.33

3.3 EFFECTS OF CROSS SECTION DISTORTION

Table A3.16 – Comparison of different boundary conditions for S12x40.8 beam with $h/t_w=40$.

$k=L_1/L$	C_b Value [Normalized with M_{cr0} ($w-inc$)]						
	SPR	TFR	QDS	HDS	TQDS	FDS	TR
0.1	1.56	1.76	1.81	1.90	2.04	2.18	2.14
0.3	1.37	2.26	2.42	2.68	2.93	3.08	3.04
0.5	1.27	2.42	2.71	3.31	3.67	3.78	3.68
0.7	1.25	1.90	2.02	2.23	2.46	2.60	2.57
0.9	1.27	1.44	1.49	1.59	1.78	1.93	1.94

Table A3.17 – Comparison of different boundary conditions for S12x40.8 beam with $h/t_w=60$.

$k=L_1/L$	C_b Value [Normalized with M_{cr0} ($w-inc$)]						
	SPR	TFR	QDS	HDS	TQDS	FDS	TR
0.1	1.43	1.54	1.57	1.64	1.78	2.03	1.97
0.3	1.32	1.87	2.01	2.27	2.64	2.91	2.85
0.5	1.22	1.94	2.14	2.62	3.43	3.59	3.48
0.7	1.19	1.65	1.75	1.96	2.28	2.54	2.48
0.9	1.18	1.30	1.34	1.41	1.61	1.90	1.89

Table A3.18 – Comparison of different boundary conditions for S12x40.8 beam with $h/t_w=80$.

$k=L_1/L$	C_b Value [Normalized with M_{cr0} ($w-inc$)]						
	SPR	TFR	QDS	HDS	TQDS	FDS	TR
0.1	1.23	1.27	1.28	1.32	1.37	1.49	1.53
0.3	1.23	1.54	1.67	1.90	2.30	2.70	2.62
0.5	1.15	1.59	1.76	2.13	3.04	3.33	3.22
0.7	1.11	1.41	1.52	1.71	2.07	2.44	2.36
0.9	1.04	1.13	1.16	1.22	1.37	1.44	1.60

Table A3.19 – Comparison of different h/t_w values for single point restraint (SPR) case.

Single Point Restraint				
$k=L_1/L$	$h/t_w=25$	$h/t_w=40$	$h/t_w=60$	$h/t_w=80$
0.1	1.62	1.56	1.43	1.23
0.3	1.36	1.37	1.32	1.23
0.5	1.26	1.27	1.22	1.15
0.7	1.26	1.25	1.19	1.11
0.9	1.31	1.27	1.18	1.04

Table A3.20 – Comparison of different h/t_w values for top flange restraint (TFR) case.

Top Flange Restraint				
$k=L_1/L$	$h/t_w=25$	$h/t_w=40$	$h/t_w=60$	$h/t_w=80$
0.1	1.93	1.76	1.54	1.27
0.3	2.56	2.26	1.87	1.54
0.5	2.90	2.42	1.94	1.59
0.7	2.09	1.90	1.65	1.41
0.9	1.54	1.44	1.30	1.13

Table A3.21 – Comparison of different h/t_w values for quarter depth stiffener (QDS) case.

Quarter Depth Stiffener				
$k=L_1/L$	$h/t_w=25$	$h/t_w=40$	$h/t_w=60$	$h/t_w=80$
0.1	2.00	1.81	1.57	1.28
0.3	2.73	2.42	2.01	1.67
0.5	3.27	2.71	2.14	1.76
0.7	2.22	2.02	1.75	1.52
0.9	1.61	1.49	1.34	1.16

Table A3.22 – Comparison of different h/t_w values for half depth stiffener (HDS) case.

Half Depth Stiffener				
$k=L_1/L$	$h/t_w=25$	$h/t_w=40$	$h/t_w=60$	$h/t_w=80$
0.1	2.09	1.90	1.64	1.32
0.3	2.92	2.68	2.27	1.90
0.5	3.61	3.31	2.62	2.13
0.7	2.38	2.23	1.96	1.71
0.9	1.72	1.59	1.41	1.22

Table A3.23 – Comparison of different h/t_w values for three quarter depth stiffener (TQDS) case.

Three Quarter Depth Stiffener				
$k=L_1/L$	$h/t_w=25$	$h/t_w=40$	$h/t_w=60$	$h/t_w=80$
0.1	2.17	2.04	1.78	1.37
0.3	3.03	2.93	2.64	2.30
0.5	3.70	3.67	3.43	3.04
0.7	2.49	2.46	2.28	2.07
0.9	1.83	1.78	1.61	1.37

Table A3.24 – Comparison of different h/t_w values for full depth stiffener (FDS) case.

Full Depth Stiffener				
$k=L_1/L$	$h/t_w=25$	$h/t_w=40$	$h/t_w=60$	$h/t_w=80$
0.1	2.23	2.18	2.03	1.49
0.3	3.10	3.08	2.91	2.70
0.5	3.76	3.78	3.59	3.33
0.7	2.56	2.60	2.54	2.44
0.9	1.90	1.93	1.90	1.44

Table A3.25 – Comparison of different h/t_w values for twist restraint (TR) case.

Twist Restraint				
$k=L_1/L$	$h/t_w=25$	$h/t_w=40$	$h/t_w=60$	$h/t_w=80$
0.1	2.21	2.14	1.97	1.53
0.3	3.07	3.04	2.85	2.62
0.5	3.68	3.68	3.48	3.22
0.7	2.54	2.57	2.48	2.36
0.9	1.91	1.94	1.89	1.60

Table A3.26 – Percent reduction in capacity for TFR case.

Top Flange Restraint			
% Reduction			
$k=L_1/L$	$h/t_w=40$	$h/t_w=60$	$h/t_w=80$
0.1	8.93	20.46	34.43
0.3	11.76	27.09	39.73
0.5	16.29	32.90	44.96
0.7	8.84	21.17	32.29
0.9	6.39	15.41	26.51

Table A3.27 – Percent reduction in capacity for QDS case.

Quarter Depth Stiffener			
% Reduction			
$k=L_1/L$	$h/t_w=40$	$h/t_w=60$	$h/t_w=80$
0.1	9.48	21.32	35.86
0.3	11.43	26.46	38.79
0.5	17.34	34.51	46.12
0.7	9.03	21.16	31.69
0.9	7.63	17.05	28.00

Table A3.28 – Percent reduction in capacity for HDS case.

Half Depth Stiffener			
% Reduction			
$k=L_1/L$	$h/t_w=40$	$h/t_w=60$	$h/t_w=80$
0.1	9.00	21.60	37.02
0.3	8.01	22.12	34.98
0.5	8.18	27.28	41.02
0.7	6.34	17.75	28.26
0.9	7.49	17.93	29.20

Table A3.29 – Percent reduction in capacity for TQDS case.

Three Quarter Depth Stiffener			
% Reduction			
$k=L_1/L$	$h/t_w=40$	$h/t_w=60$	$h/t_w=80$
0.1	6.02	18.13	37.10
0.3	3.29	12.84	24.34
0.5	0.70	7.23	17.81
0.7	1.49	8.61	17.13
0.9	3.11	12.08	25.08

Table A3.30 – Percent reduction in capacity for FDS case.

Full Depth Stiffener			
% Reduction			
$k=L_1/L$	$h/t_w=40$	$h/t_w=60$	$h/t_w=80$
0.1	2.30	8.73	<i>Loc.Bck.</i>
0.3	0.67	6.04	13.07
0.5	0.38	4.69	11.51
0.7	1.64	0.70	4.37
0.9	1.81	0.39	<i>Loc.Bck.</i>

Table A3.31 – Percent reduction in capacity for TR case.

Twist Restraint			
% Reduction			
$k=L_1/L$	$h/t_w=40$	$h/t_w=60$	$h/t_w=80$
0.1	3.13	11.07	<i>Loc.Bck.</i>
0.3	1.20	7.21	14.65
0.5	0.12	5.58	12.62
0.7	1.01	2.43	7.31
0.9	1.27	1.31	<i>Loc.Bck.</i>

Table A3.32 – Percent reduction values for TFR, QDS and HDS cases.

	$k=L_1/L$	$h/t_w=40$	$h/t_w=60$	$h/t_w=80$
Top Flange Restraint	0.1	8.93	20.46	34.43
	0.3	11.76	27.09	39.73
	0.5	16.29	32.90	44.96
	0.7	8.84	21.17	32.29
	0.9	6.39	15.41	26.51
Quarter Depth Stiffener	0.1	9.48	21.32	35.86
	0.3	11.43	26.46	38.79
	0.5	17.34	34.51	46.12
	0.7	9.03	21.16	31.69
	0.9	7.63	17.05	28.00
Half Depth Stiffener	0.1	9.00	21.60	37.02
	0.3	8.01	22.12	34.98
	0.5	8.18	27.28	41.02
	0.7	6.34	17.75	28.26
	0.9	7.49	17.93	29.20
Reduction Factor (Eqn. 3.4)	0.1	10.20	23.80	37.40
	0.3	12.68	29.58	46.48
	0.5	13.20	30.80	48.40
	0.7	11.78	27.48	43.18
	0.9	8.40	19.60	30.80
Reduction Factor (Eqn. 3.5)	0.1	17.50	32.50	47.50
	0.3	17.50	32.50	47.50
	0.5	17.50	32.50	47.50
	0.7	17.50	32.50	47.50
	0.9	17.50	32.50	47.50

Table A3.33 – Percent reduction values for TQDS case.

	$k=L_1/L$	$h/t_w=40$	$h/t_w=60$	$h/t_w=80$
Three Quarter Depth Stiffener	0.1	6.02	18.13	37.10
	0.3	3.29	12.84	24.34
	0.5	0.70	7.23	17.81
	0.7	1.49	8.61	17.13
	0.9	3.11	12.08	25.08
Reduction Factor (Eqn. 3.6)	0.1	10.50	24.50	38.50
	0.3	6.86	16.01	25.16
	0.5	5.10	11.90	18.70
	0.7	5.21	12.16	19.11
	0.9	7.20	16.80	26.40

CHAPTER 4 – ANALYSIS OF A DOUBLE OVERHANGING MONORAIL

4.1 COMPARISON OF SINGLE AND DOUBLE OVERHANGING BEAMS

Table A4.2 – Comparison of single and double overhanging beams for TFR case.

	$k=L_1/L$	$h/t_w=25$		$h/t_w=40$		$h/t_w=60$		$h/t_w=80$	
		SOH	DOH	SOH	DOH	SOH	DOH	SOH	DOH
		Top Flange Restraint	0.1	1.93	1.94	1.76	1.74	1.54	1.49
0.3	2.56		2.59	2.26	2.26	1.87	1.83	1.54	1.48
0.5	2.90		2.90	2.42	2.42	1.94	1.91	1.59	1.53
0.7	2.09		2.09	1.90	1.91	1.65	1.65	1.41	1.38
0.9	1.54		1.59	1.44	1.51	1.30	1.32	1.13	0.87

Table A4.3 – Comparison of single and double overhanging beams for QDS case.

	$k=L_1/L$	$h/t_w=25$		$h/t_w=40$		$h/t_w=60$		$h/t_w=80$	
		SOH	DOH	SOH	DOH	SOH	DOH	SOH	DOH
		Quarter Depth Stiffener	0.1	2.00	2.02	1.81	1.80	1.57	1.53
0.3	2.73		2.80	2.42	2.43	2.01	1.97	1.67	1.59
0.5	3.27		3.27	2.71	2.71	2.14	2.11	1.76	1.68
0.7	2.22		2.22	2.02	2.03	1.75	1.76	1.52	1.50
0.9	1.61		1.64	1.49	1.56	1.34	1.41	1.16	1.09

Table A4.4 – Comparison of single and double overhanging beams for HDS case.

	$k=L_1/L$	$h/t_w=25$		$h/t_w=40$		$h/t_w=60$		$h/t_w=80$	
		SOH	DOH	SOH	DOH	SOH	DOH	SOH	DOH
		Half Depth Stiffener	0.1	2.09	2.14	1.90	1.93	1.64	1.63
0.3	2.92		3.03	2.68	2.76	2.27	2.29	1.90	1.85
0.5	3.61		3.63	3.31	3.31	2.62	2.61	2.13	2.07
0.7	2.38		2.38	2.23	2.23	1.96	1.97	1.71	1.73
0.9	1.72		1.72	1.59	1.64	1.41	1.52	1.22	1.32

Table A4.5 – Comparison of single and double overhanging beams for TQDS case.

	$k=L_1/L$	$h/t_w=25$		$h/t_w=40$		$h/t_w=60$		$h/t_w=80$	
		SOH	DOH	SOH	DOH	SOH	DOH	SOH	DOH
		Three Quarter Depth Stiffener	0.1	2.17	2.24	2.04	2.10	1.78	1.82
0.3	3.03		3.19	2.93	3.11	2.64	2.79	2.30	2.40
0.5	3.70		3.76	3.67	3.73	3.43	3.46	3.04	3.04
0.7	2.49		2.50	2.46	2.46	2.28	2.28	2.07	2.07
0.9	1.83		1.82	1.78	1.78	1.61	1.66	1.37	1.43

Table A4.6 – Comparison of single and double overhanging beams for FDS case.

	$k=L_1/L$	$h/t_w=25$		$h/t_w=40$		$h/t_w=60$		$h/t_w=80$	
		SOH	DOH	SOH	DOH	SOH	DOH	SOH	DOH
Full Depth Stiffener	0.1	2.23	2.32	2.18	2.28	2.03	2.15	1.49	1.50
	0.3	3.10	3.29	3.08	3.32	2.91	3.20	2.70	3.01
	0.5	3.76	3.84	3.78	3.89	3.59	3.74	3.33	3.51
	0.7	2.56	2.57	2.60	2.62	2.54	2.56	2.44	2.47
	0.9	1.90	1.89	1.93	1.93	1.90	1.90	1.44	1.46

Table A4.7 – Comparison of single and double overhanging beams for TR case.

	$k=L_1/L$	$h/t_w=25$		$h/t_w=40$		$h/t_w=60$		$h/t_w=80$	
		SOH	DOH	SOH	DOH	SOH	DOH	SOH	DOH
Twist Restraint	0.1	2.21	2.28	2.14	2.22	1.97	2.05	1.53	1.55
	0.3	3.07	3.24	3.04	3.25	2.85	3.11	2.62	2.90
	0.5	3.68	3.77	3.68	3.79	3.48	3.62	3.22	3.37
	0.7	2.54	2.56	2.57	2.59	2.48	2.50	2.36	2.38
	0.9	1.91	1.92	1.94	1.94	1.89	1.89	1.60	1.48